NTNU

Norwegian University of
Science and Technology

Methods for Identification of Instantaneous Frequencies for Application in Isolated Microgrid

Haakon Jondal Helle

Master of Science in Cybernetics and Robotics
Submission date: June 2017
Supervisor: Marta Maria Cabrera Molinas, ITK
Co-supervisor: Mohammad Amin, ITK

Norwegian University of Science and Technology
Department of Engineering Cybernetics

Problem Description

Name:	Haakon Jondal Helle
Faculty:	Faculty of Information Technology and Electrical Engineering
Department:	Department of Engineering Cybernetics
Study program:	Cybernetics and robotics (Master, 5 years)
Main profile:	Control of smart grids and renewable energy
Start date:	9 January 2017
Due date:	5 June 2017
Supervisor:	Professor Marta Molinas

Title: Methods for Identification of Instantaneous Frequencies for Application in Isolated Microgrids

Work Description:

- Find a suitable model for the extended Kalman filter and unscented Kalman filter for estimating ”instantaneous frequencies” or time-varying frequencies in multicomponent signals.
- Implement an Extended Kalman filter and an unscented Kalman filter using this model, in Matlab and Simulink.
- Assess the strengths and limitations of this model when identifying instantaneous frequencies in synthetic signals.
- Implement Hilbert Huang Transform (empirical mode decomposition and Hilbert Transform) in Matlab and Simulink.
- Propose the method of merging empirical mode decomposition and Kalman filtering. Suggest structures for single-phase and three-phase systems. Validate the merged tool using synthetic signals.
- Assess the aforementioned methods with real voltage measurements from a marine vessel power system. Implement a phase-locked loop to serve as reference for the tracking of the fundamental frequency.

Abstract

THE introduction of new methods for production and distribution of electrical energy has increased the attention related to problems with power quality and the presence of time-varying frequencies. It has been reported several cases with such problems in isolated electrical systems such as isolated microgrids for incorporation of renewable energy sources and marine vessel power systems. The sources and loads in such systems are usually interfaced with power electronic equipment, meaning that there is low or no inertia. The low inertia and the stochastic nature of the generation and loads results in systems that are prone to nonlinear distortions and variations in the fundamental frequency. The hitherto used measurement- and monitoring equipment have mostly been based on average value calculation. The aforementioned problems in isolated electrical systems have made the need of measurement of instantaneous values instead of average values apparent, in order to have monitoring- and control systems with satisfying performance and accuracy.

This thesis studies the use of several types of Kalman filters (KF), Hilbert-Huang Transform (HHT) and the proposed method of merging empirical mode decomposition (EMD) and KF for the purpose of tracking instantaneous values of voltage- and current waveforms in isolated microgrids with the aforementioned challenges. Both synthetic signals and real measurements from a marine vessel power system were used to validate the methods. The algorithms and methods were implemented in Matlab and Simulink.

In varying degrees, the methods did all prove to be viable options for tracking of the fundamental frequency on the marine vessel. The proposed method turned out to be particularly powerful to decompose multicomponent signals consisting of several time-varying monocomponents, and track their instantaneous amplitude and frequency.

Sammendrag

INNFØRINGEN av nye metoder for produksjon og fordeling av elektrisk energi har økt oppmerksomheten rundt problemer med strømkvalitet og tidsvarierende frekvenser. Det har blitt rapportert flere hendelser med slike problemer i isolerte kraftsystem som for eksempel isolerte microgrids for inkorporering av fornybare energikilder og kraftsystem ombord på marinfartøy med elektrisk fremdrift. Kilder og laster i slike system er vanligvis knyttet sammen gjennom kraftelektronisk utstyr, noe som fører til lavt treghetsmoment. Det lave treghetsmomentet, i tillegg til kraftproduksjonens og lastenes stokastiske natur, resulterer i system som er utsatt for ulineære forvrengninger og variasjoner i grunnfrekvensen. Det hittil benyttede måle- og overvåkingsutstyret har for det meste vært basert på gjennom- snittsverdi beregninger. De tidligere nevnte problemene i isolerte kraftsystem har gjort det tydelig at målinger heller burde baseres på momentanverdier, slik at overvåkings- og kontrollsystemer opprettholder tilfredsstillende ytelse og nøyaktighet.

Denne masteroppgaven studerer bruken av forskjellige Kalman-filtre (KF), Hilbert-Huang Transform (HHT) og den foreslåtte metoden for sammenslåing av empirical mode decomposition (EMD) og KF for følging av momentantverdier i spennings- og strøm bølgeformer i isolerte microgrids med de nevnte utfordringene. Både syntetiske signaler og ekte spenningsmålinger fra et kraftystem på marinfartøy ble brukt til å validere de forskjellige metodene. Algoritmene og metodene ble implementert i Matlab og Simulink.

I varierende grad, viste de foreslåtte metodene seg å være gode metoder for følging av grunnfrekvensen om bord på marinfartøyet. Den foreslåtte metoden viste seg å være spesielt kraftig for å dekomponere signal bestende av flere tidsvarierende monokomponenter, og estimere deres momentane amplitude og frekvens.

Preface

THIS is the master's thesis to conclude the Master of Science degree in Cybernetics and Robotics at the Norwegian University of Science and Technology. The work was carried out at the Department of Engineering Cybernetics during spring 2017.

I would like to express my sincere gratitude to my supervisor, professor Marta Molinas for giving me the opportunity to work with such an interesting topic. The completion of the thesis would not have been possible without her tireless guidance and her remarkable insight on the topic. Secondly, I would like to thank Vijay Venu Vadlamudi. His great lectures aroused my interest for the world of electric power engineering.

I am grateful for the mail conversations with Manuel Duarte Ortigueira and Raul Rato for increasing my understanding of their version of the EMD.

I would also like to thank Tomasz Tarasiuk from Gdynia Maritime Institute for providing the measurements from the marine vessel power system.

Trondheim, 5 June 2017

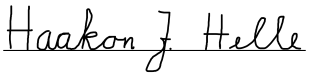

Haakon Jondal Helle

Table of Contents

List of Tables

List of Figures

Abbreviations

AC	Alternating current
AKF	Adaptive Kalman filter
DC	Direct current
DFT	Discrete Fourier transform
EKF	Extended Kalman filter
EMD	Empirical mode decomposition
FFT	Fast Fourier transform
FIR	Finite impulse response
HHT	Hilbert-Huang transform
HT	Hilbert transform
IMF	Intrinsic mode function
PV	Photovoltaics
KF	Kalman filter
MAF	Moving average filter
MMC	Modular multilevel converter
PI	Proportional-Integral
PLL	Phase-locked loop
RMS	Root mean square
THD	Total harmonic distortion
UKF	Unscented Kalman filter

Chapter 1

Introduction

1.1 Background and Motivation

DUE to a large amount of rotating masses in the electric generators and loads, classical electric power systems have been characterized by excellent power quality and frequency with very small drifts away from the fundamental frequency, usually at $50\,Hz$ or $60\,Hz$. With the increasing amount of power electronics equipment in the grids, such as rectifiers, inverters, adjustable speed drives and the like, harmonics and nonlinear distortions are increasingly injected. This makes real-time measurement and estimation of essential quantities such as frequency and magnitude a challenging, but necessary task. With no connections to a strong-/stiff grid, stand-alone power systems such as isolated microgrids (e.g photovoltaics (PV) microgrids or marine vessel power systems) are prone to problems with severe frequency deviations. The low inertia in such systems requires properly implemented controllers in order to maintain satisfying operation. In addition to the harmonic pollution, advanced inverter control may produce time-varying oscillations in conditions with varying load demand [1]. The role of these invertes are to serve as an interface between the generation source and the loads. "Static" power electronics equipment such as the inverter is a means of inverting DC power to AC power in the cases where the generation source is not rotating, e.g solar panels, fuel cells or battery banks supplying DC power [1]. Hitherto, data acquisition- and measurement systems have generally been based on average value calculations and harmonics that are integer multiples of a constant fundamental frequency [2, 3]. After an extensive study of IEC Standard 61000-4-7 measuring methods, [4] states that these methods do not produce accurate results in environments with time-varying angular frequency. Keeping the aforementioned problems of nonlinearities and time-varying quantities in mind, measurements and estimation in isolated microgrids should rather be based on instantaneous amplitude and frequency rather than the usage of average values [1, 5]. With improved data acquisition- and measurement tools, the supervisory control systems in isolated microgrids may perform better actions, and earlier hidden distortions may be revealed.

1.2 Thesis Objective and Scope of Work

THE objective of this thesis is to review current literature on specific frequency identification methods, and assess their viability in microgrids with time-varying fundamental frequency and nonlinear distortions. This is obtained by running simulations using synthetic signals and real voltage measurements from a marine vessel power system.

Fundamental theory for microgrids and the methods used in this thesis are carried out in a thorough manner. The extended Kalman filter (EKF) and unscented Kalman filter (UKF) algorithms, and their models are derived. Also a phase-locked loop (PLL), EMD, Hilbert transform (HT) and the proposed method of merging EMD and UKF are outlined. These methods are implemented in Matlab and Simulink for assessment of their potential for tracking of instantaneous amplitude and frequency of voltage- and current waveforms in isolated microgrids, and for verification of the derived models used by the EKF and UKF. It is also studied how some of the methods are able to break down multicomponent signals into monocomponents, from which instantaneous amplitude and frequency with physical meaning can be studied. Synthetic signals and real voltage measurements from a marine vessel power system during sea voyage will be used for this purpose.

1.3 Main Contributions

THE main contributions of this thesis are:

- An extensive literature review of papers and books relevant to the objective is rendered in an easy-to-read and compact thesis.
- A proposed method for better phase angle estimation in noisy environments.
- Study of the nonlinear KF model limitations, regarding tracking of signals with time-varying amplitude and frequency.
- The merging of EMD and KF is in this thesis proposed by the supervisor and author, for the first time to the authors knowledge. Single-phase and three-phase topologies are developed. This new method is tested with synthetic signals and real voltage measurements, showing promising results.

1.4 Structure of the Report

THE thesis is outlined as follows:
Chapter 1: Introduction - This chapter presents the background and motivation for the work in this thesis. It also contains the thesis objective, scope of work, main contributions and the structure of the report.
Chapter 2: State-of-the-art in Methods for Frequency Identification in Microgrids - This chapter introduces the concept of microgrids, fundamental definitions and important frequency identification methods. It also contains literature review and state-of-the-art within the field.

Chapter 3: Summary of Previous Work - This chapter summarizes the most important results from the specialization project carried out autumn 2016.
Chapter 4: Harmonics- and Frequency Tracking using Kalman Filters - Linear and nonlinear mathematical models for the different KFs are developed. Simulations are conducted to confirm the models and to study their feasibility.
Chapter 5: Merging Empirical Mode Decomposition and Kalman Filtering - The proposed method of combining EMD and KF is outlined, and validated with simulations.
Chapter 6: Assessment of Methods for Tracking of Time-Varying Frequencies in a Marine Vessel Power System - The feasibility of the different frequency identification methods outlined in this thesis are assessed by using real voltage measurements from a marine vessel power system during sea voyage in rough sea conditions.
Chapter 7: Conclusion & Future Work - Conclusion of the thesis and recommended work for future papers and master theses.
Appendix A: Simulink Models - Some of the Simulink models used in this thesis are included in this appendix.
Appendix B: Matlab Code - Some of the scripts and functions used in Matlab and Simulink are listed here.

Chapter 2

State-of-the-art in Methods for Frequency Identification in Microgrids

2.1 Introduction to Microgrids

ACCORDING to the U.S Department of Energy a microgrid is ”a group of interconnected loads and distributed energy resources with clearly defined electrical boundaries that acts as a single controllable entity with respect to the grid and can connect and disconnect from the grid to enable it to operate in both grid connected or island modes” [6]. The International Energy Agency (IEA) estimates that to achieve the goal of universal access to electrical energy, 70% of rural areas lacking electricity will have to connect to mini-grid or off-grid solutions [7]. Often microgrids are intended as a means of incorporating distributed and renewable energy sources such as solar PV, wind power, small hydro and more. Microgrids are also used for military applications, offshore and maritime applications. Figure 2.1, inspired by [8], shows an example DC microgrid with a PV array and battery bank supplying DC and AC loads. The microgrid is able to connect to and disconnect from the main grid. This point is called the point of common coupling (PCC). When operating in island mode the available capacity from the energy storage and PV array must exceed the power drawn from critical loads. Should there be any surplus energy in the microgrid, it may be sent to the main grid or be stored in the battery bank. The AC/DC block is a rectifier/inverter, depending on the direction of the power flow. The DC/DC blocks are mainly buck or boost converters, depending on whether the voltage levels should decrease or increase. The DC/DC block connected to the battery bank is a so-called bi-directional converter, having the ability to increase or decrease the voltage levels depending on the direction of the power flow.

Though having many advantages, there are several challenges related to the microgrids. In isolated microgrids the amount of rotating mass is usually low, i.e low inertia. This can often lead to severe frequency deviations if the controllers are not properly implemented [9].

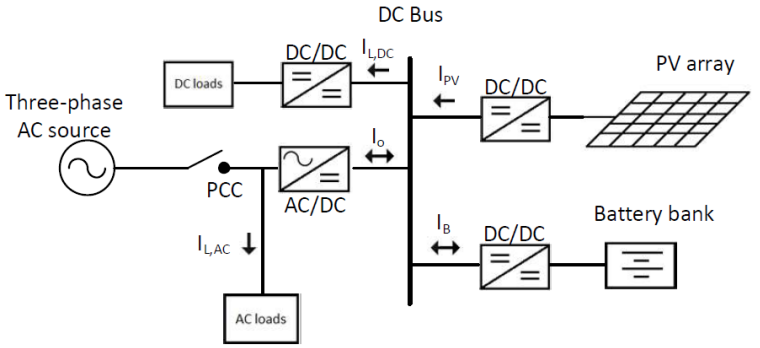

Figure 2.1: An example microgrid with DC bus and the possibility to connect to the main grid.

2.2 Fundamental Definitions

In the following subsections several fundamental terms and definitions used in the thesis are explained, containing basic three-phase system and circuit analysis theory, harmonics, Fourier analysis, different transformations and more.

2.2.1 Time- and Phasor Domain

Balanced three-phase voltages are shown in the time- and phasor domain in Figure 2.2 and Figure 2.3. The three phases are denoted a,b and c, and can be represented as in equation (2.1). The three phases are displaced by $120°$ or $\frac{2\pi}{3}$ radians in balanced systems, and has the frequency f_n, usually $50\,Hz$ or $60\,Hz$ in most power systems. Currents will have the same waveforms as the voltages.

$$v_a(t) = \hat{V}_a \cos(2\pi f_n t) \tag{2.1a}$$

$$v_b(t) = \hat{V}_b \cos(2\pi f_n t - 120°) \tag{2.1b}$$

$$v_c(t) = \hat{V}_c \cos(2\pi f_n t + 120°) \tag{2.1c}$$

Line voltages, or line-line voltages may be expressed as $v_{ab}(t) = v_a(t) - v_b(t)$ and so on. Phase- and line voltages are often denoted as v_ϕ and v_l. The following relations applies:

$$v_l = \sqrt{3} v_\phi \angle 30° \tag{2.2}$$

Three-phase quantities may also be represented in the phasor domain:

$$\mathbf{V}_a = \hat{V}_a e^{j0°} = \hat{V}_a \angle 0° \tag{2.3a}$$

$$\mathbf{V}_b = \hat{V}_b e^{-j120^\circ} = \hat{V}_b \angle -120^\circ \tag{2.3b}$$

$$\mathbf{V}_c = \hat{V}_c e^{j120^\circ} = \hat{V}_c \angle 120^\circ \tag{2.3c}$$

where the the angular frequency $\omega_n = 2\pi f_n$ is assumed to be known. In fact each phasor is multiplied with the term $e^{j\omega_n t}$, but is usually omitted as it is implied.

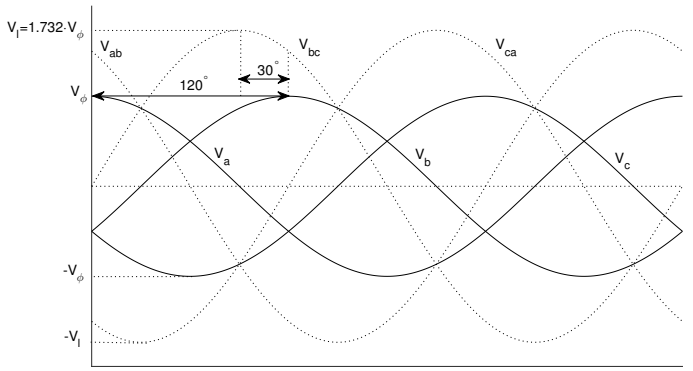

Figure 2.2: Three-phase voltages in the time domain. Phase voltages plotted with solid lines and line voltages plotted with dotted lines.

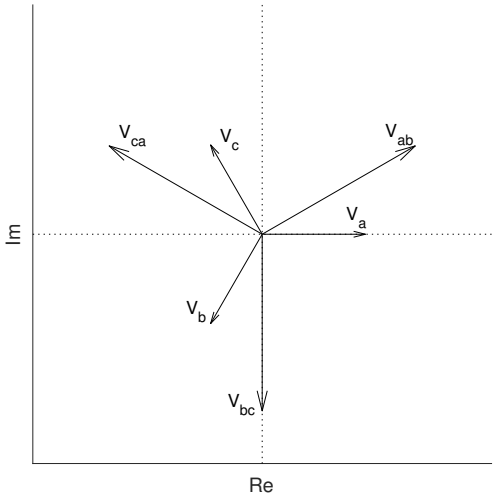

Figure 2.3: Three-phase voltages shown in a phasor diagram.

2.2.2 RMS, Effective Value

The term root mean square (RMS) is commonly used in electrical power engineering. V_{rms} is the effective value of v(t), it can be regarded as the DC-value that will give the same dissipated power over an resistance as $v(t)$ does on average [10]. The instantaneous power over an resistance can be expressed as:

$$p(t) = v(t)i(t) = \frac{v(t)^2}{R} \tag{2.4}$$

The RMS value of any voltage can be found by an integral, as in (2.5).

$$\frac{V_{RMS}^2}{R} = \frac{1}{R}\frac{1}{T}\int_0^T v(t)^2 dt \tag{2.5}$$

giving

$$V_{RMS} = \sqrt{\frac{1}{T}\int_0^T v(t)^2 dt} \tag{2.6}$$

For sinusoids, it can be shown that $\hat{V} = \sqrt{2}V_{RMS}$.

2.2.3 Harmonics and Total Harmonic Distortion

Total harmonic distortion (THD) is a measure of harmonic distortion, and is defined as the ratio between the sum of the power of the harmonics and the power of the fundamental frequency. Harmonic components are often introduced by power electronics equipment, such as rectifiers and inverters, and has frequencies with an integer times the fundamental frequency. Let a distorted voltage be defined as:

$$v_s(t) = v_{s1}(t) + \sum_{h\neq 1} v_{sh}(t), \tag{2.7}$$

where $v_{s1}(t)$ is the fundamental component and $v_{sh}(t)$ are the harmonics. In terms of RMS, the THD of the voltage defined in equation (2.7) can be found as follows [10]:

$$\%THD_v = 100 \cdot \frac{\sqrt{V_s^2 - V_{s1}^2}}{V_{s1}} = 100 \cdot \sqrt{\sum_{h\neq 1}\left(\frac{V_{sh}}{V_{s1}}\right)^2} \tag{2.8}$$

2.2.4 Fourier Analysis

Fourier analysis of electrical voltage and current waveforms is hitherto the most widely used method in instrumentation for electrical applications such as smart meters, spectrum analyser, phasor measurement units and many more. With the presence of time-varying quantities the frequency based methods may suffer from the leakage and picket-fence effects [11]. Leakage refers to the spreading of energy from one frequency to the adjacent frequencies. The picket-fence effect occurs if the analysed signal contains harmonics that are not an integer times the fundamental.

According to IEEE 519 and IEC 61000-4-7, harmonic measurements using Fourier series should be done in the following manner [2, 3, 12]:

$$x(t) = a_0 + \sum_{h=1}^{\infty} c_h \sin(\frac{h}{N}\omega_n t + \phi_h) \tag{2.9a}$$

$$c_h = \sqrt{a_h^2 + b_h^2} \tag{2.9b}$$

$$\phi_h = \tan^{-1}\left(\frac{a_h}{b_h}\right), \text{ if } b_h \geq 0 \tag{2.9c}$$

$$\phi_h = \pi + \tan^{-1}\left(\frac{a_h}{b_h}\right), \text{ if } b_h < 0 \tag{2.9d}$$

and

$$a_h = \frac{2}{T_w}\int_0^{T_w} x(t)\cos\left(\frac{h}{N}\omega_n t + \phi_h\right)\ dt \tag{2.10a}$$

$$b_h = \frac{2}{T_w}\int_0^{T_w} x(t)\sin\left(\frac{h}{N}\omega_n t + \phi_h\right)\ dt \tag{2.10b}$$

$$a_0 = \frac{1}{T_w}\int_0^{T_w} x(t)\ dt \tag{2.10c}$$

where w_n is the fundamental frequency, h is the harmonic order, T_w is the duration of the window and N is the number of fundamental periods within the window width. As the measurements obtained by data acquisition- and measurement systems are in discrete time, the equations above is not used exactly as they are given. The aforementioned transforms DFT and FFT are in that case used, where the only difference between the two is that the latter is a more efficient implementation. The FFT takes advantage of symmetries, reducing the number of computing operations needed from $\mathcal{O}(N^2)$ (DFT) to $\mathcal{O}(N \log N)$ (FFT) [13].

2.2.5 Clarke Transformation

The Clarke transformation, also known as $\alpha\beta\gamma$-, or $\alpha\beta 0$ transformation, is a means of simplifying three-phase quantities by projecting them onto a stationary reference frame denoted α and β [14]. This transformation is conceptually similar to the Park-, or $dq0$ transformation, where the difference is that the Park transformation projects three-phase quantities onto a rotating reference frame. The transformation from abc reference frame to the stationary reference frame, α and β, can be obtained by:

$$X_{\alpha\beta 0} = TX_{abc}, \tag{2.11}$$

and inversely from $\alpha\beta 0$ to abc:

$$X_{abc} = T^{-1}X_{\alpha\beta 0}. \tag{2.12}$$

The transformation matrices in equation (2.11) and (2.12) are defined as in (2.13) and (2.14).

$$T = \frac{2}{3}\begin{bmatrix} 1 & -\frac{1}{2} & -\frac{1}{2} \\ 0 & \frac{\sqrt{3}}{2} & -\frac{\sqrt{3}}{2} \\ \frac{1}{2} & \frac{1}{2} & \frac{1}{2} \end{bmatrix} \tag{2.13}$$

$$T^{-1} = \begin{bmatrix} 1 & 0 & 1 \\ -\frac{1}{2} & \frac{\sqrt{3}}{2} & 1 \\ -\frac{1}{2} & -\frac{\sqrt{3}}{2} & 1 \end{bmatrix} \tag{2.14}$$

The transformation is shown in Figure 2.4, where balanced three phase quantities are transformed into the $\alpha-$ and β axis. Since the system is balanced, the γ or 0 component equals zero.

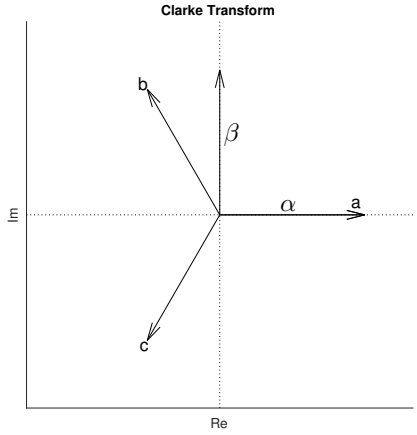

Figure 2.4: The Clarke transformation shown graphically.

2.2.6 Symmetrical Component Theory - Fortescue's Theorem

The fundamentals for symmetrical component theory was first presented by Fortescue in [15], which is a paper that is by many seen upon as one of the most important papers in electric power engineering. Fortescue proposed that any set of N unbalanced phasors could be expressed as the sum of N symmetrical sets of balanced phasors. This does of course apply to three phase system, where the three symmetrical sets of balanced phasors are called positive-, negative- and zero sequence components. The positive sequence components is a set of three balanced vectors, with equal magnitude, same phase sequence and displaced by $120°$ with respect to each other. The same properties applies to the negative sequence components except that the phase sequence is opposite. The zero sequence components is a set of three balanced vectors with equal magnitudes and equal phase angles, i.e in phase.

Any set of unbalanced voltages or currents in the abc reference frame, X_{abc}, can be transformed into balanced positive, neqative and zero sequence components, X_{012}. $X_{012} = A^{-1}X_{abc}$, where A^{-1} is the transformation matrix:

$$A^{-1} = \frac{1}{3}\begin{bmatrix} 1 & 1 & 1 \\ 1 & a & a^2 \\ 1 & a^2 & a \end{bmatrix}, \tag{2.15}$$

where $a = e^{j120^\circ}$. Similarly the sequence components can be transformed back to the original unbalanced quantities. X_{abc}. $X_{abc} = AX_{012}$ where A is the transformation matrix:

$$A = \begin{bmatrix} 1 & 1 & 1 \\ 1 & a^2 & a \\ 1 & a & a^2 \end{bmatrix} \tag{2.16}$$

Figure 2.5 shows an unbalanced three-phase system, whereas Figure 2.6 shows the sequence components.

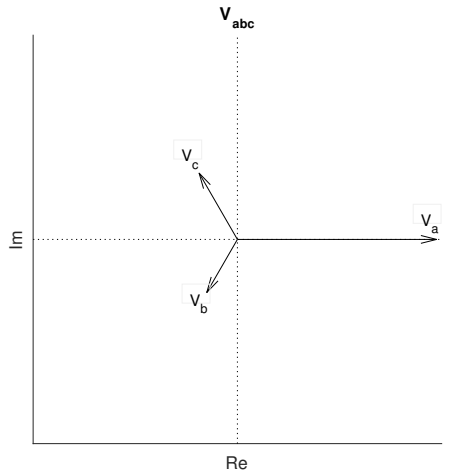

Figure 2.5: Unbalanced three phase voltages.

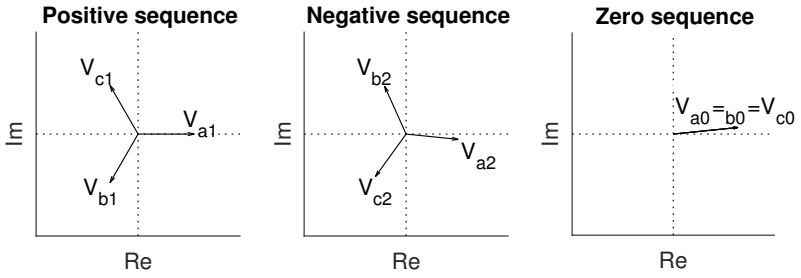

Figure 2.6: The sequence components of the unbalanced voltages.

2.3 Frequency Identification Methods

THE task of estimating frequency and other parameters in isolated microgrids is a task of grave importance, for many different reasons. The methods mentioned in section 1.2 will here be outlined. Rich literature on these methods is available, and also for other methods that will not be covered in this thesis. Some other widely used methods for on-line fundamental frequency estimation (and other parameters) are: adaptive Prony's method [16], least squares methods [17, 18], adaptive notch filtering [19, 20] and Newton type algorithms [21, 22].

2.3.1 Kalman Filter and Extended Kalman Filter

For time-domain- and model based methods, KF is a widely used tool for a variety of power system applications. The use of KF for electrical engineering purposes has been around since the early 80's [23, 24], and has been of interest in applications and research ever since. Several great approaches have been suggested for both balanced and unbalanced power system, under the assumption of both stationary- and non-stationary frequency in [11, 25–29]. Another example of usage is state estimation in electrical drives [30].

The KF has been around for over 50 years, and is still alive and well and widely used in many applications. In 1960 R. E. Kalman found a recursive solution for the Wiener filter problem, the solution was called KF and was first presented in [31]. The theory in this section is based on [32].

It is assumed that the following discrete state-space model can be used to estimate the random process:

$$x_{k+1} = A_k x_k + w_k \tag{2.17a}$$

$$y_k = C_k x_k + v_k \tag{2.17b}$$

x_k and y_k are the process state- and measurement vector at time t_k. A_k is the system matrix relating x_k to x_{k+1}, assuming there is no noise. Matrix C_k gives the noiseless relationship between the state- and measurement vector at time t_k. w_k and v_k are the model error and measurement error, assumed to be white sequences with zero mean, and normal distributed covariances $w_k \sim \mathcal{N}(0, Q_k)$ and $v_k \sim \mathcal{N}(0, R_k)$. Furthermore the covariance matrices Q_k and R_k are uncorrelated, and are uncorrelated at different time instants, as stated in (2.18).

$$E[w_k w_i^T] = \begin{cases} Q_k, \, i = k \\ \mathbf{0} =, \, i \neq k \end{cases} \quad , \tag{2.18a}$$

$$E[v_k v_i^T] = \begin{cases} R_k, \, i = k \\ \mathbf{0} =, \, i \neq k \end{cases} \quad , \tag{2.18b}$$

$$E[w_k v_i^T] = \mathbf{0}, \forall k, \, i \tag{2.18c}$$

To start the KF algorithm, an initial estimate $\hat{x}_0^-$ and its error covariance P_0^- is needed. The "hat" denotes that this is an estimate, and the superscript "-" denotes that this is the *a priori* estimate, meaning this is the best estimate before taking the measurement at time t_k into consideration. Furthermore the estimation error is defined as:

$$e_k^- = x_k - \hat{x}_k^-. \tag{2.19}$$

Assuming the estimation error in (2.19) has zero mean, the error covariance matrix is given by (2.20).

$$P_k^- = E[e_k^- e_k^{-T}] = E[(x_k - \hat{x}_k^-)(x_k - \hat{x}_k^-)^T] \tag{2.20}$$

We now want to improve our a priori estimate, $\hat{x}_k^-$, by using the measurement y_k. The *a posteriori* estimate $\hat{x}_k$ can be found by:

$$\hat{x}_k = \hat{x}_k^- + K_k(y_k - C_k \hat{x}_k^-). \tag{2.21}$$

K_k is the yet to be determined Kalman gain, with the purpose of giving an optimal updated estimate through properly weighting the measurement residual $y_k - \hat{y}_k$ and adding it to the a priori estimate. The a posteriori estimate results in the following error covariance matrix:

$$P_k = E[e_k e_k^T] = E[(x_k - \hat{x}_k)(x_k - \hat{x}_k)^T]. \tag{2.22}$$

The purpose of the Kalman gain K_k, and the KF itself, is to minimize the individual terms along the major diagonal of P_k. It can be shown that (2.23) minimizes the mean-square estimation error.

$$K_k = P_k^- C_k^T (C_k P_k^- C_k^T + R_k)^{-1} \tag{2.23}$$

For optimal gain conditions the error covariance matrix for the updated estimate is given as:

$$P_k = (I - K_k C_k) P_k^- \tag{2.24}$$

The a priori estimate for the next time step, t_{k+1}, can be found by simply projecting $\hat{x}_k$ ahead via the system matrix A_k, as given in (2.25).

$$\hat{x}_{k+1}^- = A_k \hat{x}_k \tag{2.25}$$

The error covariance matrix for the next time step is given by:

$$P_{k+1}^{-} = E[e_{k+1}^{-} e_{k+1}^{-T}] = A_k P_k A_k^T + Q_k \tag{2.26}$$

For the case of systems with highly nonlinear characteristics , the KF will normally behave badly and the EKF may be a better candidate. Assuming the state-space model is on the form:

$$\dot{x} = f(x,t) + w \tag{2.27a}$$

$$y = h(x,t) + v \tag{2.27b}$$

To obtain the state transition matrix, A_k, and measurement matrix, C_k, at time step k equation (2.28) and (2.29) are used.

$$A_k = \left.\frac{\partial f}{\partial x}\right|_{\hat{x}_k} \tag{2.28}$$

$$C_k = \left.\frac{\partial h}{\partial x}\right|_{\hat{x}_k} \tag{2.29}$$

Though the above equations may seem abstract at first, the goal of the KF is quite simple. It is simply a computer algorithm that processes discrete measurements into optimal estimates. Figure 2.7 shows the KF loop visually, and summarizes equations (2.21)-(2.26).

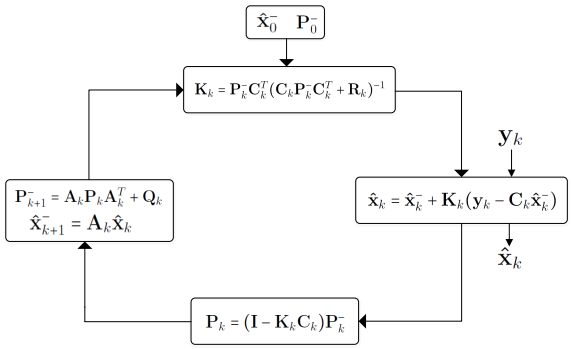

Figure 2.7: The KF algorithm.

2.3.2 The Unscented Kalman Filter

For nonlinear systems, the EKF is the most widely used state estimation algorithm. It has low complexity and is easy to implement. Though the EKF possess many advantages, such as simple tuning, it also falls short when compared to other nonlinear state estimation algorithms, mostly due to linearization errors and the need of calculating derivatives [33] [34]. The theory in this part is based on [33] and [35].

Assume we have a n-dimensional state-space model as given in (2.30):

$$x_{k+1} = f(x_k, t_k) + w_k \tag{2.30a}$$

$$y_k = h(h_k, t_k) + v_k \tag{2.30b}$$

$$w_k \sim (0, Q_k) \tag{2.30c}$$

$$v_k \sim (0, R_k) \tag{2.30d}$$

The UKF is initalized:

$$\hat{x}_0 = E[x_0] \tag{2.31a}$$

$$P_0 = [e_k e_k^T] = E[(x_0 - \hat{x}_0)(x_0 - \hat{x}_0)^T] \tag{2.31b}$$

As opposed to the EKF which uses linearized models to propagate from time step $k-1$ to k, the UKF picks a minimal set of sigma points around the mean, which is further propagated through the nonlinear functions, meaning it is derivative free. This is known as the unscented transformation, which results in a new mean and covariance estimate. The unscented transformation is based on the idea that it is easy to perform nonlinear transformations on single points. By using Cholesky factorization to find matrix square roots, i.e $\left(\sqrt{nP}\right)^T \sqrt{nP} = nP$, the sigma points are defined as follows:

$$\chi_{k-1}^{(i)} = \hat{x}_{k-1} + \tilde{x}^{(i)}, \qquad i = 1, ..., 2n \tag{2.32a}$$

$$\tilde{x}^{(i)} = \left(\sqrt{nP_{k-1}}\right)_i^T, \qquad i = 1, ..., n \tag{2.32b}$$

$$\tilde{x}^{(n+i)} = -\left(\sqrt{nP_{k-1}}\right)_i^T, \qquad i = 1, ..., n \tag{2.32c}$$

The sigma points are then propagated through the nonlinear function $f(\cdot)$, making the vector $\chi_k^{(i)}$:

$$\chi_k^{(i)} = f(\chi_{k-1}^{(i)}, u_k, t_k) \tag{2.33}$$

The elements of $\chi_k^{(i)}$ are then combined, serving as the *a priori* estimate at time k.

$$\hat{x}_k^- = \frac{1}{2n} \sum_{i=1}^{2n} \chi_k^{(i)} \tag{2.34}$$

The *a priori* error covariance is defined as in (2.35), where it should be noted that Q_{k-1} is added to take model error into account.

$$P_k^- = \frac{1}{2n} \sum_{i=1}^{2n} (\chi_k^{(i)} - \hat{x}_k^-)(\chi_k^{(i)} - \hat{x}_k^-)^T + Q_{k-1} \tag{2.35}$$

The equations defined above are usually denoted as the time update equations. The measurement update equations are yet to be defined. Equation (2.36) defines new sigma points using the current best estimates, in fact $\hat{x}_k^-$ and P_k^-. To save computational effort one may omit the calculation of new sigma points, if one is willing to sacrifice accuracy, that is.

$$\chi_k^{(i)} = \hat{x}_k^- + \tilde{x}^{(i)}, \qquad i = 1, ..., 2n \tag{2.36a}$$

$$\tilde{x}^{(i)} = \left(\sqrt{nP_k^-}\right)_i^T, \qquad i = 1, ..., n \tag{2.36b}$$

$$\tilde{x}^{(n+i)} = -\left(\sqrt{nP_k^-}\right)_i^T, \qquad i = 1, ..., n \tag{2.36c}$$

The nonlinear measurement function $h(\cdot)$ is now used to transform the sigma points into vectors of predicted measurements, $\gamma_k^{(i)}$.

$$\gamma_k^{(i)} = h(\chi_k^{(i)}, t_k) \tag{2.37}$$

The vectors of predicted measurements are then combined to obtain the predicted measurement $\hat{y}_k$, as shown in (2.38).

$$\hat{y}_k = \frac{1}{2n}\sum_{i=1}^{2n}\gamma_k^{(i)} \tag{2.38}$$

Equation (2.39) defines the covariance of the predicted measurement.

$$P_y = \frac{1}{2n}\sum_{i=1}^{2n}(\gamma_k^{(i)} - \hat{y}_k)(\gamma_k^{(i)} - \hat{y}_k)^T + R_k \tag{2.39}$$

The cross covariance between $\hat{x}_k^-$ and $\hat{y}_k$ is defined as:

$$P_{xy} = \frac{1}{2n}\sum_{i=1}^{2n}(\chi_k^{(i)} - \hat{x}_k^-)(\gamma_k^{(i)} - \hat{y}_k)^T \tag{2.40}$$

The *a posteriori* estimates can now be found as in equation (2.41)

$$K_k = P_{xy}P_y^{-1} \tag{2.41a}$$

$$\hat{x}_k = \hat{x}_k^- + K_k(y_k - \hat{y}_k) \tag{2.41b}$$

$$P_k = P_k^- - K_k P_y K_k^T \tag{2.41c}$$

Using $2n + 1$ Sigma Points

[35] suggests different scaling parameters and weights for combining the sigma points into estimates. Also an additional sigma point is added, i.e $2n + 1$ sigma points. Compared to equation (2.32) the *a priori* sigma points vectors $\chi_k^{(i)}$ are now defined as:

$$\chi_{k-1}^{(0)} = \hat{x}_{k-1}, \qquad i = 0 \tag{2.42a}$$

$$\chi_{k-1}^{(i)} = \hat{x}_{k-1} + \tilde{x}^{(i)}, \qquad i = 1, ..., 2n \tag{2.42b}$$

$$\tilde{x}^{(i)} = \left(\sqrt{(n+\lambda)P_{k-1}}\right)_i^T, \qquad i = 1, ..., n \tag{2.42c}$$

$$\tilde{x}^{(n+i)} = -\left(\sqrt{(n+\lambda)P_{k-1}}\right)_i^T, \qquad i = 1, ..., n \tag{2.42d}$$

$\chi_{k-1}^{(i)}$ will be on the form:

$$\chi_{k-1}^{(i)} = \begin{bmatrix} \hat{x}_{k-1} & \hat{x}_{k-1} + \left(\sqrt{(n+\lambda)P_{k-1}}\right)^T & \hat{x}_{k-1} - \left(\sqrt{(n+\lambda)P_{k-1}}\right)^T \end{bmatrix} \tag{2.43}$$

The scaling parameter λ is defined as in equation (2.44):

$$\lambda = \alpha^2(n + \kappa) - n, \tag{2.44}$$

where α determines the spread of the sigma points around the mean $\bar{x} = \hat{x}_{k-1}$, usually set to a small positive value, e.g 1e-3. κ is a secondary scaling parameter, usually set to 0. Then a set of mean and covariance weights are defined as in equation (2.45):

$$\omega_0^{(m)} = \frac{\lambda}{n+\lambda} \tag{2.45a}$$

$$\omega_0^{(c)} = \frac{\lambda}{n+\lambda} + (1 - \alpha^2 + \beta) \tag{2.45b}$$

$$\omega_i^{(m)} = \omega_i^{(c)} = \frac{1}{2(n+\lambda)}, \qquad i = 1, ..., 2n \tag{2.45c}$$

β is used to incorporate prior knowledge about the probabilistic distribution, e.g $\beta = 2$ for Gaussian distribution. The different state, measurement and covariance estimates are now found as:

$$\hat{x}_k^- = \sum_{i=0}^{2n} \omega_m^{(i)} \chi_k^{(i)} \tag{2.46a}$$

$$\hat{y}_k = \sum_{i=0}^{2n} \omega_m^{(i)} \gamma_k^{(i)} \tag{2.46b}$$

$$P_k^- = \sum_{i=0}^{2n} \omega_c^{(i)} (\chi_k^{(i)} - \hat{x}_k^-)(\chi_k^{(i)} - \hat{x}_k^-)^T + Q_{k-1} \tag{2.46c}$$

$$P_y = \sum_{i=0}^{2n} \omega_c^{(i)} (\gamma_k^{(i)} - \hat{y}_k)(\gamma_k^{(i)} - \hat{y}_k)^T + R_k \tag{2.46d}$$

$$P_{xy} = \sum_{i=0}^{2n} \omega_c^{(i)} (\chi_k^{(i)} - \hat{x}_k^-)(\gamma_k^{(i)} - \hat{y}_k)^T \tag{2.46e}$$

The above changes are also applied to the *a posteriori* estimates. The observant reader may notice that with $\lambda = 0$, equations (2.42)-(2.46) reduces to the equations from the preceding subsection.

Adaptive update of model- and measurement error covariances

[34] proposes an adaptive update of the model- and measurement error covariance matrices, in order to better respond to rapid fluctuations and varying measurement noise. Let

$$Z_k = \hat{x}_k - \hat{x}_k^- = K_k(y_k - \hat{y}_k) = \begin{bmatrix}\psi_{1k} & \psi_{2k}\end{bmatrix}^T \tag{2.47}$$

The iteratively updated model error covariance matrix is then defined as follows:

$$Q_k = \frac{1}{2}(\psi_{1k}^2 + \psi_{2k}^2) \times I_{2\times 2} \tag{2.48}$$

It can be seen that a large error in one of the states will affect the whole model. The adaptive measurement noise covariance matrix is given as:

$$R_k = \xi R_{k-1} + (1-\xi)|e_k||e_{k-1}| \tag{2.49}$$

where ξ is the forgetting factor between 0 and 1.

2.3.3 Hilbert Transform

The HT is an important tool in signal processing. It is a tool for projecting real signals onto the imaginary axis, which further makes it possible to obtain instantaneous amplitude and frequency. Let the HT of the function $x(t)$ be defined as in [36]:

$$y(t) = \mathscr{H}[x(t)] = \frac{1}{\pi} p.v \int_{-\infty}^{\infty} \frac{x(\tau)}{t-\tau} d\tau, \tag{2.50}$$

where p.v indicates the Cauchy principal value. The original signal can now be expressed in an exponential form as shown equation (2.51).

$$z(t) = x(t) + jy(t) = a(t)e^{j\theta(t)}, \tag{2.51}$$

where

$$a(t) = \sqrt{x^2(t) + y^2(t)} \tag{2.52a}$$

$$\theta(t) = \tan^{-1}\left\{\frac{y(t)}{x(t)}\right\} \tag{2.52b}$$

$a(t)$ and $\theta(t)$ are the instantaneous amplitude and phase respectively. Knowing the instantaneous phase, the instantaneous frequency $f(t)$ can then be found:

$$f(t) = \frac{1}{2\pi}\frac{d\theta(t)}{dt} \tag{2.53}$$

The notions of instantaneous amplitude and frequency for general signals are not well-defined [5, 37]. For a perfect sinusoid, the instantaneous frequency will be $f = \frac{1}{T}$. Figure 2.8 compares the HT and FFT applied to a signal with varying amplitude and frequency, given as:

$$x(t) = \begin{cases}\cos(2\pi 3t), & 0 \le t < 2.5 \\ 0.5 \cdot \cos(2\pi 6t), & 2.5 \le t \le 10\end{cases} \tag{2.54}$$

It can be seen that the Fourier transform struggles when analysing signals with time-varying components, and is representing the signal energy as a leakage around $3\,Hz$ and $6\,Hz$, whereas the instantaneous amplitude and frequency found from the HT quickly settles to the correct values.

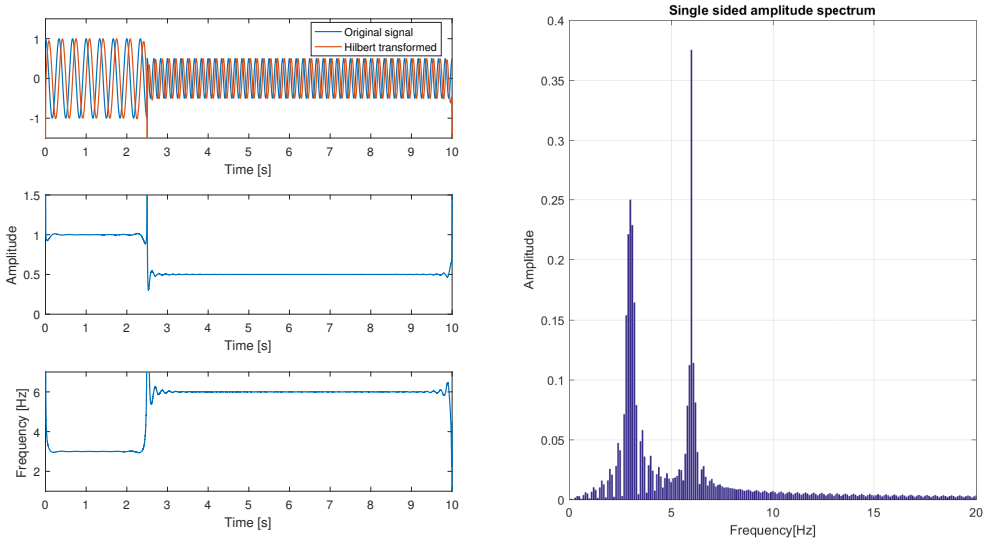

(a) HT **(b)** FFT

Figure 2.8: Comparison between the HT and FFT.

2.3.4 Hilbert-Huang Transform

The HHT, in fact a NASA designated name, combines EMD and the aforementioned HT, and is well suited for analysis of non-stationary signals. The use of HHT has proven useful for obtaining instantaneous amplitude, frequency and power in power systems and isolated microgrids [1, 5, 38, 39]. As will be outlined in the next subsection, the EMD decomposes signals into monocomponents/IMFs. From the IMFs it is possible to obtain instantaneous amplitudes and frequencies, as the monocomponents often can be regarded as near periodic and near sinusoidal [5, 37]. The amount of IMFs greatly varies depending on the signal at hand. Knowing the IMFs of a signal one may reveal important information, e.g oscillatory modes. EMD is originally an offline method, but there are also examples of on-line EMD implementations [40–42]. To realize the HHT for real-time applications, a FIR filter can be used to estimate the HT, as in [43–45].

Empirical Mode Decomposition - The Sifting Process

The EMD and sifting process aims to extract IMF from non-stationary and nonlinear data in a systematic manner. [46] states that an IMF must satisfy the following conditions:

- The number of extrema and the number of zero crossings must either be equal or differ at most by one

- At any point, the average value of the envelopes defined by the local maxima and by the local minima is zero.

The EMD starts by finding all the local maxima and minima of the signal $x(t)$. The extrema points are connected by cubic spline interpolation lines as shown in Figure 2.9. The average of the upper and lower spline envelopes is computed and here denoted as m_1. The mean is subtracted from the original signal [46]:

$$h_1 = x(t) - m_1 \tag{2.55}$$

Further, the extrema points of h_1 are identified and again connected by cubic spline interpolation lines. The new mean is defined as m_{11}. This so called sifting procedure is repeated k times until h_{1k} is an IMF or the standard deviation, SD, computed from two consecutive sifting is below a certain value, typically 0.2 or 0.3 [46] .

$$SD = \sum_{t=0}^{T} \left[\frac{|(h_{1(k-1)}(t) - h_{1k}(t)|^2}{h_{1(k-1)}^2(t)} \right] \tag{2.56}$$

$$h_{1k} = h_{1(k-1)} - m_{1k} \tag{2.57}$$

The first IMF is designated as

$$c_1 = h_{1k}, \tag{2.58}$$

and subtracted from the original signal, resulting in the residue r_1.

$$r_1 = x(t) - c_1 \tag{2.59}$$

The steps mentioned above are repeated until the residue is a monotonic function, or so small that it is less than a predefined value of substantial consequence. From the resulting IMFs and the last residue the signal $x(t)$ can be represented as [46]:

$$x(t) = \sum_{i=1}^{n} c_i + r_n \tag{2.60}$$

To illustrate, the signal $x(t) = \cos(2\pi 50t) + 0.5\cos(2\pi 250t) + 0.3\cos(2\pi 750t)$ is passed through the HHT. Figure 2.10 clearly shows the steps of the sifting process for the three first IMFs, while Figure 2.11 shows the instantaneous amplitudes and frequency obtained from the three first IMFs. As can be seen, the highest frequency components are extracted first.

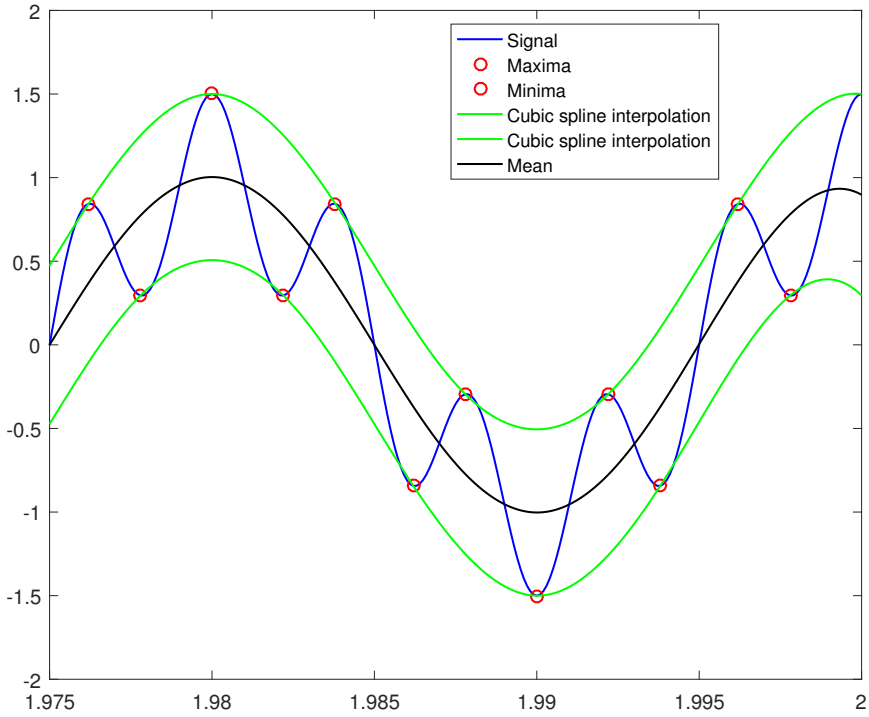

Figure 2.9: Signal with spline interpolations and mean.

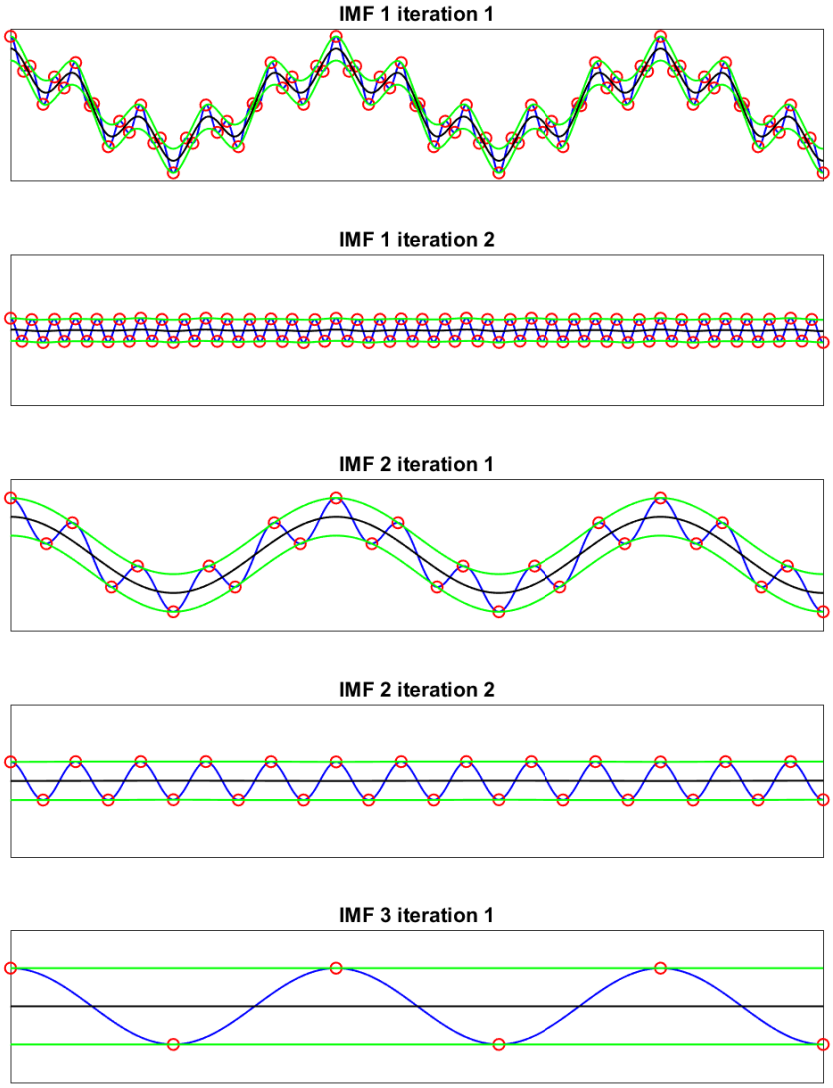

Figure 2.10: Steps of the EMD.

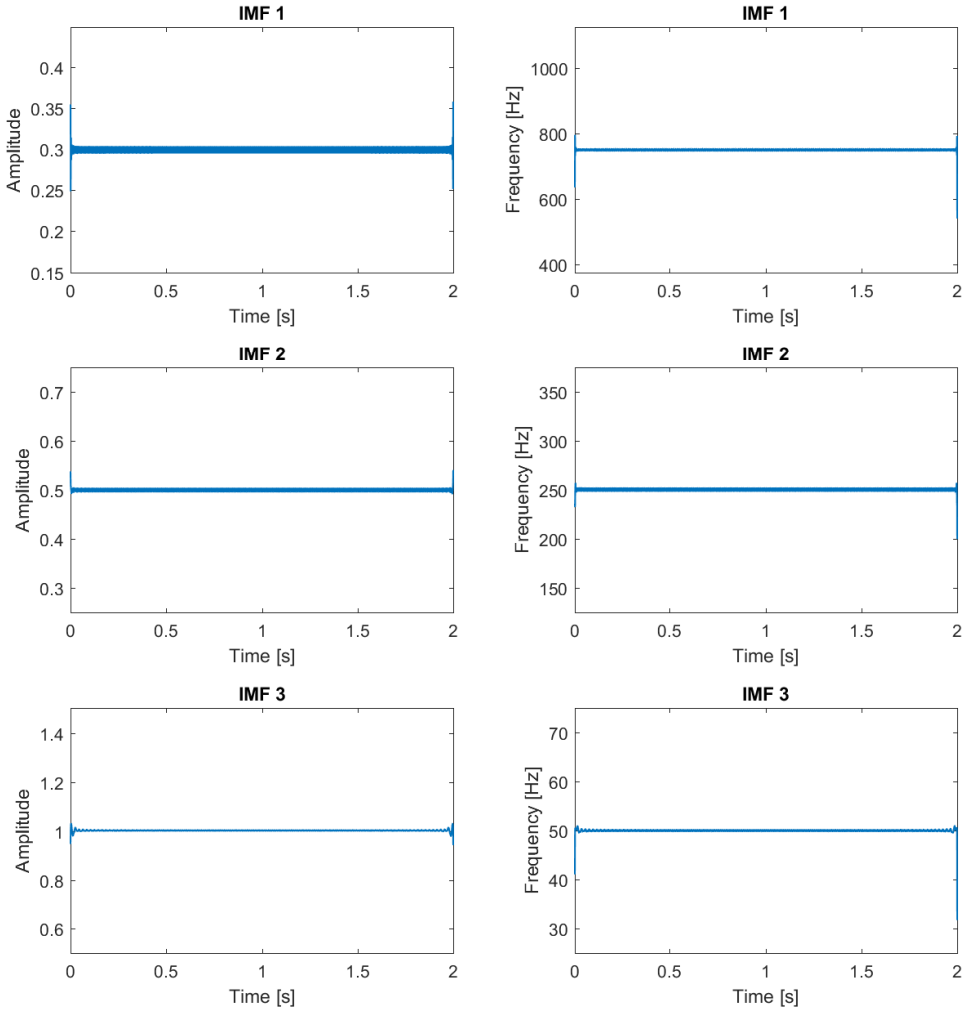

Figure 2.11: Instantaneous amplitude and frequency of the three first IMFs.

2.3.5 Phase-Locked Loop

The PLL is the state-of-the-art method for extracting the phase angle of grid voltages [47, 48]. Many versions of the PLL are implemented in the dq synchronous reference frame, as can be seen in Figure 2.12a, which is based on [49]. The estimated d- and q-axis voltages are low-pass filtered with the cut off frequency ω_{LP}. The inverse tangent of the

filtered voltages is used as input to the Proportional-Integral (PI) controller [49], giving:

$$\omega_{PLL} = \theta_v(k_p \cdot \frac{1 + T_i s}{T_i s}) + \omega_g, \tag{2.61}$$

where ω_g is the nominal grid angular frequency. A typical step response is showed in Figure 2.12b. The Park-/dq transform is given as [50]:

$$\begin{bmatrix} v_d \\ v_q \end{bmatrix} = \sqrt{\frac{2}{3}} \begin{bmatrix} \cos(\theta) & \cos(\theta - \frac{2\pi}{3}) & \cos(\theta + \frac{2\pi}{3}) \\ -\sin(\theta) & -\sin(\theta - \frac{2\pi}{3}) & -\sin(\theta + \frac{2\pi}{3}) \end{bmatrix} \begin{bmatrix} v_a \\ v_b \\ v_c \end{bmatrix} \tag{2.62}$$

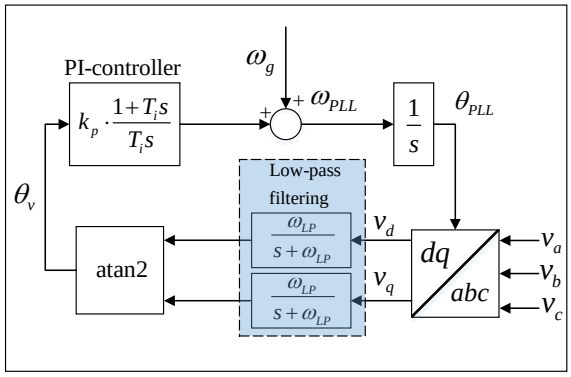

(a) Example of a PLL.

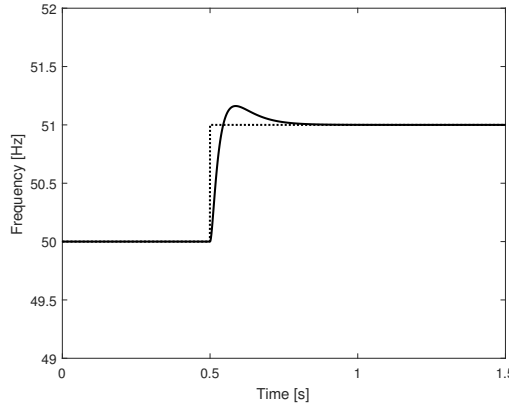

(b) Step response of the PLL.

Figure 2.12: PLL structure and step response.

Chapter 3

Summary of Previous Work

THIS thesis is a continuation of the specialization project carried out autumn 2016 at the Department of Engineering Cybernetics [51]. The specialization project mainly involved the development and testing of different types of Kalman filters for harmonics- and frequency tracking in electric power systems. This chapter includes the main results and findings of the specialization project.

3.1 The Kalman filter and the Adaptive Kalman filter

THE mathematical models for the KF, the adaptive Kalman filter (AKF) and the three-phase voltages subject to harmonic pollution are given in section 4.1. The KF and AKF were subjected to the experiment as given in table 3.1

As can be seen from Figure 3.1, the AKF outperformed the KF. This was to be expected as the AKF was designed to quickly handle fluctuations. Figure 3.2 shows the error of the KF and AKF, and also how the tuning of the AKF impacted the error. The error was defined as in equation 3.1.

$$Magnitude\,error_{dB} = 10 \cdot log\left(\sqrt{\sum_{i \in h_p \cup h_n} (|V_{i,ref}| - |V_i|)^2}\right) \tag{3.1a}$$

$$Angle\,error_{dB} = 10 \cdot log\left(\sqrt{\sum_{i \in h_p \cup h_n} (\angle V_{i,ref} - \angle V_i)^2}\right) \tag{3.1b}$$

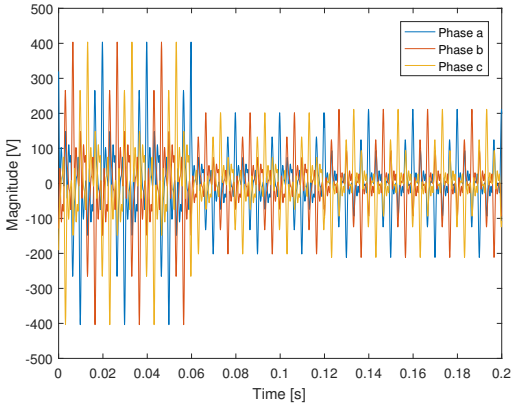

(a) Three-phase voltages in the abc frame

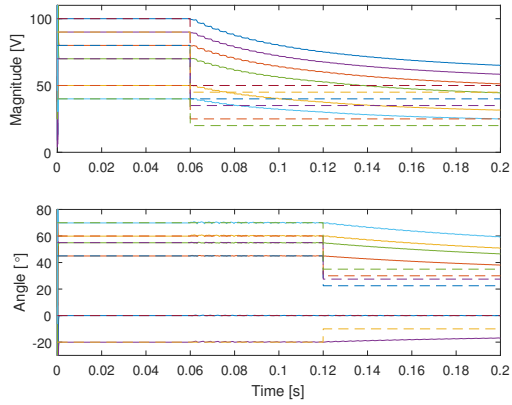

(b) KF

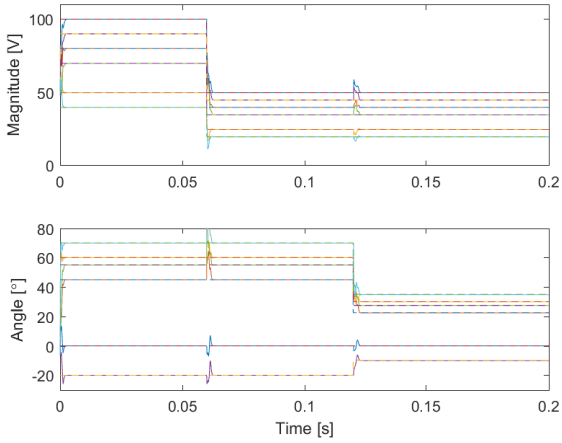

(c) AKF

Figure 3.1: The regular KF and the AKF compared.

Project experiment 1	
Parameter	**Value**
Simulation time	0.2 s
Sample time, T_s	$10^{-6}\,s$
Measurement noise, $v = v_1 = v_2$, turn on Noise mean, $E[v]$ Noise variance, $var(v) = E[v^2]$	0.08 s 0 1
Positive sequence harmonics, h_p Negative sequence harmonics, h_n	[1, 7, 13] [5, 11, 17]
$\lvert V_{i,ref}\rvert, 0\,s \leq t < 0.06\,s$ $\lvert V_{i,ref}\rvert, 0.06\,s \leq t \leq 0.2\,s$ $\angle V_{i,ref}, 0\,s \leq t < 0.12\,s$ $\angle V_{i,ref}, 0.12\,s \leq t \leq 0.2\,s$ $i \in h_p$	[100, 80, 50] [50, 40, 25] [0°, 45°, 60°] [0°, 22.5°, 30°]
$\lvert V_{j,ref}\rvert, 0\,s \leq t < 0.06\,s$ $\lvert V_{j,ref}\rvert, 0.06\,s \leq t \leq 0.2\,s$ $\angle V_{j,ref}, 0\,s \leq t < 0.12\,s$ $\angle V_{j,ref}, 0.12\,s \leq t \leq 0.2\,s$ $j \in h_n$	[90, 70, 40] [45, 35, 20] [−20°, 55°, 70°] [−10°, 27.5°, 35°]

Table 3.1: Parameters for project experiment 1.

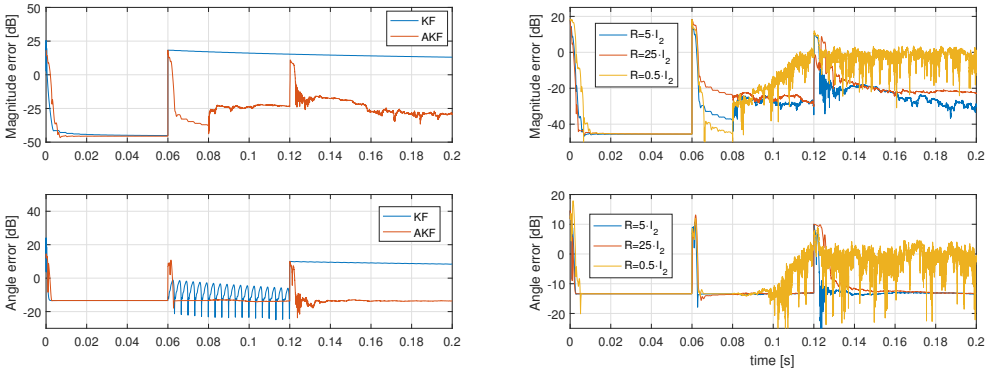

(a) KF and AKF compared.

(b) Different tunings of the AKF compared.

Figure 3.2: Comparison between the KF and the AKF.

Figure 3.3 shows the modular multilevel converter (MMC) impedance found by small-signal perturbation in a MMC-diode bridge system. This was obtained by injecting shunt currents of $0.01\,pu$ between the MMC and the diode bridge. Figure 3.4 compares the analytical impedance, and impedance obtained by FFT and KF at specified harmonics present in the system.

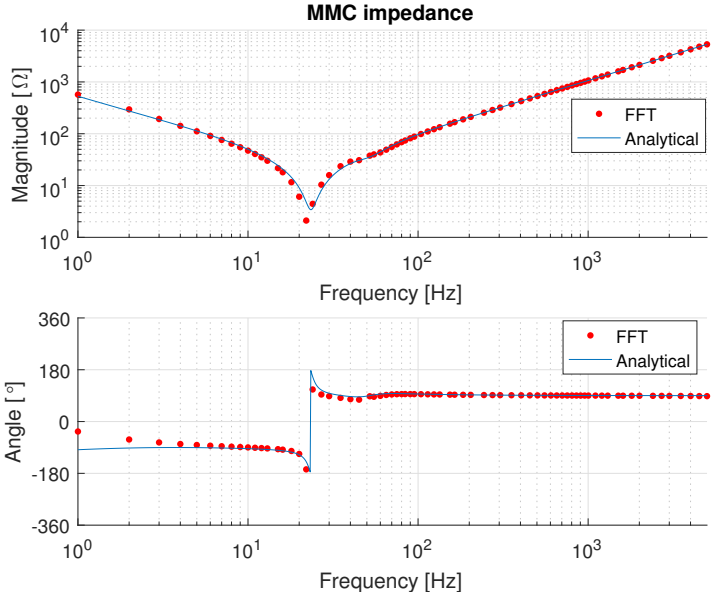

Figure 3.3: The analytical impedance of the MMC compared with impedance obtained by small-signal perturbation.

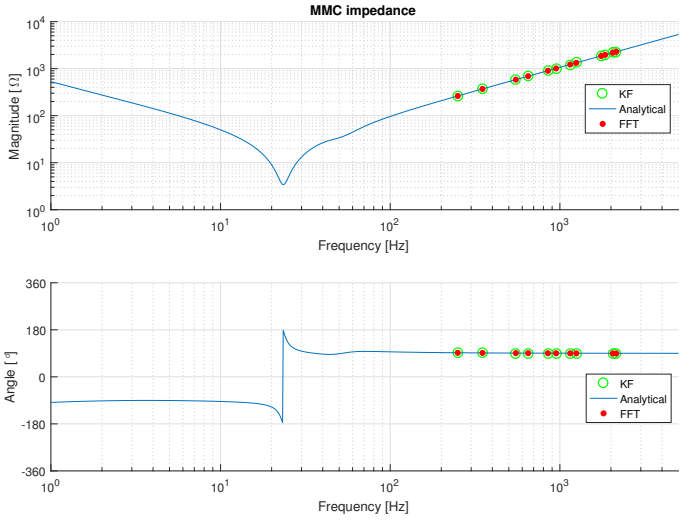

Figure 3.4: The analytical impedance of the MMC compared with impedance obtained by KF and FFT for selected harmonics.

3.2 The Extended Kalman Filter

THE equations for the model used by the EKF can be found in section 4.2. Figure 3.5 shows how the EKF was able to track the voltage magnitude and frequency as given in table 3.2. At this point the author had had no luck tracking the phase angle. It was found that the performance of the EKF was linked to the ratio between the diagonal elements of the model error covariance matrix Q, defined as $\lambda = \frac{q_{1,1}}{q_{2,2}}$.

Project experiment 2	
Parameter	**Value**
Simulation time	2 s
Sample time, T_s	$10^{-5}\ s$
Measurement noise, v, turn on Noise mean, $E[v]$ Noise variance, $var(v) = E[v^2]$	0 s 0 0.1
Positive sequence harmonics, h_p Negative sequence harmonics, h_n	$[1]$ $\emptyset$
$\lvert V_{i,ref}\rvert, 0\,s \leq t < 0.2\,s$ $\lvert V_{i,ref}\rvert, 0.2\,s \leq t \leq 2\,s$ $\angle V_{i,ref}, 0\,s \leq t \leq 2\,s$ $i \in h_p$	$[100]$ $[50]$ $[45°]$
$f_n, 0\,s \leq t < 0.8\,s$ $f_n, 0.8\,s \leq t \leq 2\,s$	$50\,Hz$ $51\,Hz$

Table 3.2: Parameters for project experiment 2.

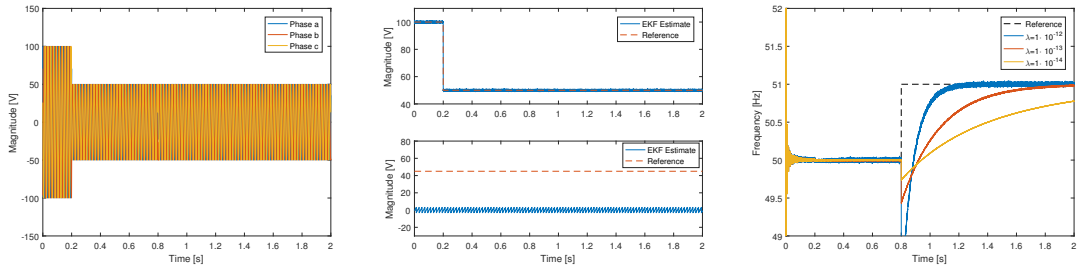

(a) Three-phase voltages in the abc frame **(b)** Magnitude and phase angle **(c)** Frequency

Figure 3.5: Simulations of the EKF.

Chapter 4

Harmonics- and Frequency Tracking Using Kalman Filters

IN this chapter two Kalman filter models will be developed, one for tracking of harmonics and one for tracking of time-varying fundamental frequency. The models will be validated by simulations.

The first model is based on [26,52], and [25] for the adaptive approach. Here it is assumed that the angular frequency ω is constant, and that the system is balanced. In addition a nonlinear model suitable for the EKF and UKF, as in [27] and [34] is developed. This model can be used to include tracking of the fundamental frequency.

4.1 Tracking of Three-Phase Harmonics Based on Linear Kalman Filter

FOR now, $\omega(t) = \omega_n$ is assumed to be known and constant. It is also assumed that the system is balanced, hence $V_a = V_b = V_c$. Equation (4.1) represents three-phase voltages in the abc frame with amplitudes $V_a\,, V_b\,, V_c$, phase angles $\phi_a\,, \phi_b\,, \phi_c$, and a known angular frequency ω_n. The angular frequency is given by $\omega_n = 2\pi f_n$, where f_n in this case is the fundamental frequency at $50\,Hz$. The model to be developed also applies for three-phase currents in the abc frame.

$$v_a(t) = V_a \cos(\omega_n t + \phi_a) \tag{4.1a}$$

$$v_b(t) = V_b \cos(\omega_n t + \phi_b) \tag{4.1b}$$

$$v_c(t) = V_c \cos(\omega_n t + \phi_c) \tag{4.1c}$$

Let $\phi_b = \phi_a - \frac{2\pi}{3}$ and $\phi_c = \phi_a + \frac{2\pi}{3}$, i.e the phases are aligned in the positive sequence. As explained in section 2.2.6, any unbalanced systems can be transformed into three sets of balanced phasors. The positive-, negative- and zero sequence will from now on be denoted as $p, n, 0$, respectively.

$$v_a(t) = v_{a,p}(t) + v_{a,n}(t) + v_{a,0}(t) \tag{4.2a}$$

$$v_b(t) = v_{b,p}(t) + v_{b,n}(t) + v_{b,0}(t) \tag{4.2b}$$

$$v_c(t) = v_{c,p}(t) + v_{c,n}(t) + v_{c,0}(t) \tag{4.2c}$$

Furthermore we define V_p=[$V_{a,p}$,$V_{b,p}$,$V_{c,p}$]^T, V_n=[$V_{a,n}$,$V_{b,n}$,$V_{c,n}$]^T and V_0=[$V_{a,0}$,$V_{b,0}$,$V_{c,0}$]^T as in [26]. Equation (4.1) can be rearranged as in equation (4.3).

$$\begin{bmatrix} v_a(t) \\ v_b(t) \\ v_c(t) \end{bmatrix} = V_p \begin{bmatrix} \cos(\omega_n t + \phi_p) \\ \cos(\omega_n t + \phi_p - \frac{2\pi}{3}) \\ \cos(\omega_n t + \phi_p + \frac{2\pi}{3}) \end{bmatrix} + V_n \begin{bmatrix} \cos(\omega_n t + \phi_n) \\ \cos(\omega_n t + \phi_n + \frac{2\pi}{3}) \\ \cos(\omega_n t + \phi_n - \frac{2\pi}{3}) \end{bmatrix} + V_0 \begin{bmatrix} \cos(\phi_0) \\ \cos(\phi_0) \\ \cos(\phi_0) \end{bmatrix}, \tag{4.3}$$

where ϕ_p, ϕ_n, ϕ_0 are the phase angles for each sequence. Further the voltages in the abc frame are transformed into the $\alpha\beta 0$ frame using the Clarke transform, where the transformation matrix T is given in (4.4) and (4.5).

$$T = \frac{2}{3} \begin{bmatrix} 1 & -\frac{1}{2} & -\frac{1}{2} \\ 0 & \frac{\sqrt{3}}{2} & -\frac{\sqrt{3}}{2} \\ \frac{1}{2} & \frac{1}{2} & \frac{1}{2} \end{bmatrix} \tag{4.4}$$

By assuming we have a balanced system, the "0"-component is omitted and we get:

$$T = \frac{2}{3} \begin{bmatrix} 1 & -\frac{1}{2} & -\frac{1}{2} \\ 0 & \frac{\sqrt{3}}{2} & -\frac{\sqrt{3}}{2} \end{bmatrix} \tag{4.5}$$

Multiplying (4.5) with every part of (4.3) yields:

$$v_{\alpha\beta}(t) = T v_{abc}(t) = T V_p \begin{bmatrix} \cos(\omega_n t + \phi_p) \\ \sin(\omega_n t + \phi_p) \end{bmatrix} + T V_n \begin{bmatrix} \cos(\omega_n t + \phi_n) \\ -\sin(\omega_n t + \phi_n) \end{bmatrix} \tag{4.6}$$

To obtain a more convenient structure, the trigonometric theorem of addition and subtraction, as in (4.7) is used.

$$\sin(a \pm b) = \sin(a)\cos(b) \pm \cos(a)\sin(b) \tag{4.7a}$$

$$\cos(a \pm b) = \cos(a)\cos(b) \mp \sin(a)\sin(b) \tag{4.7b}$$

Applying (4.7) to (4.6):

$$\begin{bmatrix} v_\alpha(t) \\ v_\beta(t) \end{bmatrix} = \begin{bmatrix} \cos(\omega_n t) & -\sin(\omega_n t) \\ \sin(\omega_n t) & \cos(\omega_n t) \end{bmatrix} \begin{bmatrix} V_p \cos(\phi_p) \\ V_p \sin(\phi_p) \end{bmatrix} + \begin{bmatrix} \cos(\omega_n t) & -\sin(\omega_n t) \\ -\sin(\omega_n t) & -\cos(\omega_n t) \end{bmatrix} \begin{bmatrix} V_n \cos(\phi_n) \\ V_n \sin(\phi_n) \end{bmatrix} \tag{4.8}$$

In (4.9) the model is restated as a discrete state-space model fitting the KF, where i takes the values of the positive harmonic set h_p and negative harmonic set h_n, $x_{i,1}$ and $x_{i,2}$ are the α and β components at harmonic i, ω_n is the grid angular frequency, T_s is the sampling period and subscript "k" denotes the time instant. It is also assumed random walk for the states.

$$\begin{bmatrix} x_{i,1} \\ x_{i,2} \end{bmatrix}_{k+1} = \begin{bmatrix} 1 & 0 \\ 0 & 1 \end{bmatrix} \begin{bmatrix} x_{i,1} \\ x_{i,2} \end{bmatrix}_k + \begin{bmatrix} w_{i,1} \\ w_{i,2} \end{bmatrix}_k \tag{4.9a}$$

$$\begin{aligned} y_k = \begin{bmatrix} v_\alpha \\ v_\beta \end{bmatrix}_k &= \sum_{i \in h_p} \begin{bmatrix} \cos(i\omega_n k T_s) & -\sin(i\omega_n k T_s) \\ \sin(i\omega_n k T_s) & \cos(i\omega_n k T_s) \end{bmatrix} \begin{bmatrix} x_{i,1} \\ x_{i,2} \end{bmatrix}_k \\ + \sum_{i \in h_n} \begin{bmatrix} \cos(i\omega_n k T_s) & -\sin(i\omega_n k T_s) \\ \sin(i\omega_n k T_s) & \cos(i\omega_n k T_s) \end{bmatrix} \begin{bmatrix} x_{i,1} \\ x_{i,2} \end{bmatrix}_k &+ \begin{bmatrix} v_{i,1} \\ v_{i,2} \end{bmatrix}_k \end{aligned} \tag{4.9b}$$

Let the number of harmonics in the set h_p and h_n be n_p and n_n, and furthermore the total number of harmonics $N = n_p + n_n$. The total number of states will be $2N$. The model error covariance matrix, Q_k, will be a $2N \times 2N$ matrix. The measurement noise covariance matrix, R_k will be a 2×2 matrix. The system matrix A_k, and measurement matrix C_k will be matrices with dimensions $2N \times 2N$ and $2 \times 2N$ respectively. The amplitude and phase at harmonic i is found by:

$$|V_i| = \sqrt{x_{i,1}^2 + x_{i,2}^2} \tag{4.10a}$$

$$\phi_i = tan^{-1} \left\{ \frac{x_{i,2}}{x_{i,1}} \right\} \tag{4.10b}$$

The self-tuning AKF algorithm from [25] is adopted and slightly modified to include several harmonics. The AKF is implemented so that the model error covariance matrix is adaptively updated, to handle fast fluctuations in the studied signal. The model error $\hat{w}_k$ can be estimated as:

$$\begin{aligned} \hat{w}_k &= \hat{x}_k - \hat{x}_k^- = \hat{x}_k^- + K_k(y_k - C_k \hat{x}_k^-) - \hat{x}_k^- \\ &= K_k(y_k - C_k \hat{x}_k^-). \end{aligned} \tag{4.11}$$

Inspired by the algorithm in [25], the diagonal terms of the model error covariance matrix takes the value of the average of the sum of $(\hat{w}_{i,1}^2 + \hat{w}_{i,2}^2)$ for every harmonic i in the set $h_p \cup h_n$, as in (4.12) and (4.13):

$$q_k = \frac{1}{2N} \sum_{i \in h_p \cup h_n} (\hat{w}_{i,1}^2 + \hat{w}_{i,2}^2)_k \tag{4.12}$$

$$Q_k = q_k I \tag{4.13}$$

The AKF algorithm is given in Algorithm 1.

Algorithm 1 Adaptive Kalman filter algorithm for time instant $k = 0, 1, ...$

$q_k^- = Q_k(1,1)$
for $i = 1$ to N_{max_iter} **do**
  $P_k = A_k P_k^- A_k^T + Q_k$
  $K_k = P_k C_k^T (C_k P_k C_k^T + R_k)^{-1}$
  $\hat{x}_k = \hat{x}_k^- + K_k(y_k - C_k \hat{x}_k^-)$
  $\hat{w}_k = K_k(y_k - C_k \hat{x}_k^-)$
  $q_k = \frac{1}{2N} \sum_i (\hat{w}_{i,1}^2 + \hat{w}_{i,2}^2)_k$, $i \in h_p \cup h_n$
  $Q_k = q_k I$
  if $|\sqrt{q_k} - \sqrt{q_k^-}| < \epsilon$ **then**
    break
  end if
  $q_k^- = q_k$
end for
$\hat{x}_{k+1}^- = A_k \hat{x}_k$
$P_{k+1}^- = (I - K_k C_k) P_k$
$Q_{k+1} = Q_k$

4.2 Tracking of Fundamental Frequency Based on Extended- and Unscented Kalman Filter

In this section a model suitable for the EKF and UKF for frequency tracking will be developed, as in [27] and [34]. Again, balanced conditions are assumed, i.e $V_a = V_b = V_c$. The three-phase voltages $v_{abc,k}$ are described in a discrete manner:

$$v_{a,k} = V_a \cos(\omega k T_s + \phi_a) \tag{4.14a}$$

$$v_{b,k} = V_b \cos(\omega k T_s + \phi_b) \tag{4.14b}$$

$$v_{c,k} = V_c \cos(\omega k T_s + \phi_c), \tag{4.14c}$$

where k is the sampling instant, T_s is the sampling period, and $\phi_a = \phi_b + \frac{2\pi}{3} = \phi_c - \frac{2\pi}{3}$ are the phase angles aligned in the positive sequence. With the assumption of a balanced system, v_{abc} is transformed into the $\alpha\beta$ frame:

$$\begin{bmatrix} v_\alpha \\ v_\beta \end{bmatrix}_k = T v_{abc,k} = \frac{2}{3} \begin{bmatrix} 1 & -\frac{1}{2} & -\frac{1}{2} \\ 0 & \frac{\sqrt{3}}{2} & -\frac{\sqrt{3}}{2} \end{bmatrix} \begin{bmatrix} V_a \cos(\omega k T_s + \phi_a) \\ V_b \cos(\omega k T_s + \phi_b) \\ V_c \cos(\omega k T_s + \phi_c) \end{bmatrix} \tag{4.15}$$

Expressing (4.15) as a complex voltage v_k:

$$v_k = v_{\alpha,k} + j v_{\beta,k} = V_k \cos(\omega k T_s + \phi_k) + V_k j \sin(\omega k T_s + \phi_k) = V_k e^{j(\omega k T_s + \phi_k)} \tag{4.16}$$

This can further be represented in state-space form as:

$$\begin{bmatrix} x_1 \\ x_2 \end{bmatrix}_{k+1} = f(x_k) = \begin{bmatrix} x_1 \\ x_1 x_2 \end{bmatrix}_k \tag{4.17a}$$

$$y_k = v_k = h(x_k) = x_{2,k} \tag{4.17b}$$

where $x_{1,k} = x_{1,k+1} = e^{j\omega T_s}$, $x_{2,k} = V_k e^{j(\omega k T_s + \phi_k)}$ and $x_{2,k+1} = x_{1,k} x_{2,k} = e^{j\omega T_s} V_k e^{j(\omega k T_s + \phi_k)} = V_k e^{j(\omega (k+1) T_s + \phi_k)}$. For tracking of a single sinusoidal v_s, HT can be used as in [43]. The measurement equation is then given as in (4.18) . The HT can be realized with a finite impulse response (FIR) filter, both analog and digital as further explained in [44] and [45].

$$v_k = v_{s,k} + j\mathscr{H}[v_{s,k}] \tag{4.18}$$

The state-space equations in (4.17) are clearly nonlinear, hence the need for an EKF or UKF. In the case of the EKF we have to linearize around the a posteriori estimate for $\hat{x}_k$ which yields:

$$A_k = \left.\frac{\partial f}{\partial x}\right|_{\hat{x}_k} = \begin{bmatrix} 1 & 0 \\ \hat{x}_2 & \hat{x}_1 \end{bmatrix}_k \tag{4.19}$$

$$C_k = \left.\frac{\partial h}{\partial x}\right|_{\hat{x}_k} = \begin{bmatrix} 0 & 1 \end{bmatrix} \tag{4.20}$$

The UKF may use equations (4.17) directly. The magnitude, phase angle and frequency of the fundamental component are found by information from the estimated states $\hat{x}_{1,k}$ and $\hat{x}_{2,k}$ as in (4.21):

$$V_k = \sqrt{\hat{x}_{2,k} \cdot \hat{x}_{2,k}^*} \tag{4.21a}$$

$$\phi_k = Im\left\{ ln\left(\frac{\hat{x}_{2,k}}{\sqrt{\hat{x}_{2,k} \cdot \hat{x}_{2,k}^*}} \right) \right\} - k \cdot Im\left\{ ln(\hat{x}_{1,k}) \right\} \tag{4.21b}$$

$$f_k = \frac{1}{2\pi T_s} Im\left\{ ln(\hat{x}_{1,k}) \right\} \tag{4.21c}$$

The calculation of the phase angle ϕ_k is very sensitive to noise, and will quickly diverge in noisy conditions. This comes from the the last part of equation (4.21b), i.e

$$- k \cdot Im\left\{ ln(\hat{x}_{1,k}) \right\} \tag{4.22}$$

which can be rewritten as

$$- k \cdot 2\pi f_k T_s. \tag{4.23}$$

The first part of equation (4.21b) represents the angle of the rotating voltage vector, i.e

$$Im\left\{ ln\left(\frac{\hat{x}_{2,k}}{\sqrt{\hat{x}_{2,k} \cdot \hat{x}_{2,k}^*}} \right) \right\} = \sin^{-1}\left\{ Im(\frac{x_{2,k}}{\sqrt{\hat{x}_{2,k} \cdot \hat{x}_{2,k}^*}}) \right\} \tag{4.24}$$

Equation (4.22) and (4.23) represents the subtraction of how far the vector has rotated, calculated with the current frequency estimate. In noisy environments the calculation of equation (4.22) and (4.23) will be unaccurate. Hence a moving average filter is used to smoothen the frequency estimate. In this thesis a 800 sample moving average filter will be used. An n sample MAF is expressed as in (4.25).

$$f_{MAF} = \frac{1}{n} \sum_{i=0}^{n-1} f_{k-i} \tag{4.25}$$

Using f_{MAF} in equation (4.23) results in the new calculation of the phase angle:

$$\phi_k = Im\left\{ ln\left(\frac{\hat{x}_{2,k}}{\sqrt{\hat{x}_{2,k} \cdot \hat{x}_{2,k}^*}} \right) \right\} - k \cdot 2\pi f_{MAF} T_s \tag{4.26}$$

4.3 Simulations

THIS section aims to show the capabilites of the EKF and UKF for tracking of magnitude, phase angle and frequency of voltages with varying quality. The Kalman filters are first subjected to voltages with steps in magnitude, phase angle and frequency. Further the Kalman filters are subjected to voltages with time-varying amplitude and frequency. Simulink models of the experiment setup are included in Appendix A.1, and EKF and UKF code in Appendix B.4 and Appendix B.5.

4.3.1 Estimation of the Phase Angle

As can be seen in Figure 3.5, the author was not able to correctly extract the phase angle during the specialization project carried out autumn 2016. Figure 4.2 shows how the EKF is able to efficiently estimate the magnitude, phase angle and frequency of the three-phase voltages shown in Figure 4.1. Note that this is in a noise free environment, hence an aggressively tuned EKF with $q_{1,1} = 10^{-6}$, $q_{2,2} = 10^{4}$, $R = 1$. A less aggressive tuning must have been chosen in a noisy environment. It should be noted that the transient period of the frequency, and consequently the transient period of the phase angle would have increased with a less aggressive tuning. Figure 4.2 shows how the computation of the frequency and phase angle are coupled, while the magnitude is unaffected. Figure 4.3 clearly shows the difference between the original phase extraction as in [27, 34], and the phase obtained by using the proposed method, when noise is added.

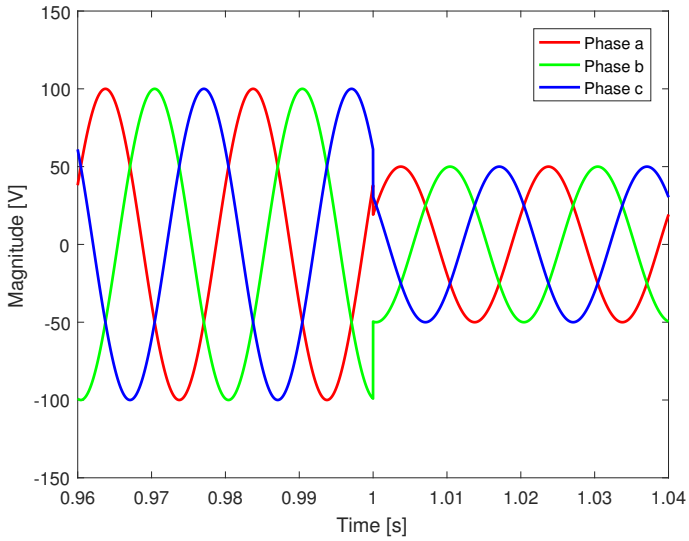

Figure 4.1: A small section of the three-phase voltages.

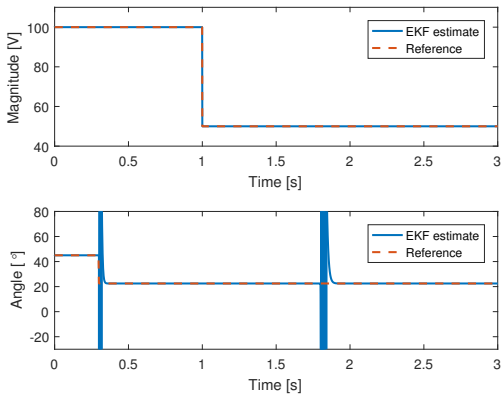

(a) Magnitude and phase angle.

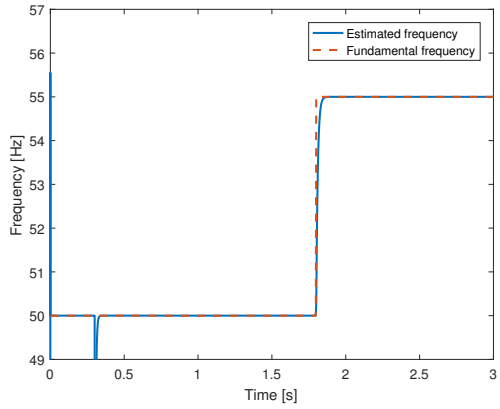

(b) Frequency.

Figure 4.2: Simulations of the EKF, no noise.

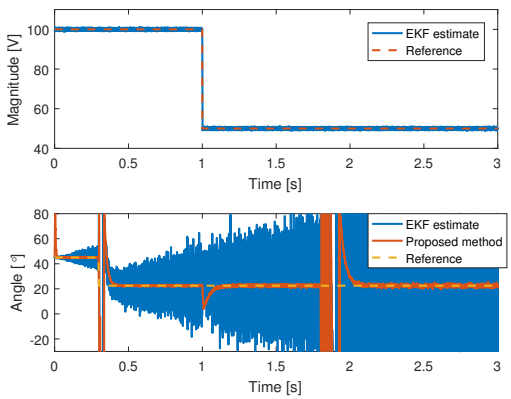

(a) Magnitude and phase angle.

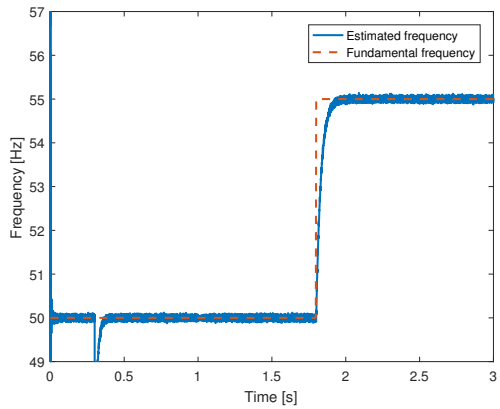

(b) Frequency.

Figure 4.3: Simulations of the EKF, with noise.

4.3.2 Tracking of Time-Varying- Amplitude and Fundamental Frequency

In this section it is studied how the UKF and EKF are managing the task of tracking voltages with time-varying amplitude and fundamental frequency. The different filters are subjected to three-phase voltages with amplitudes and frequencies as in equation (4.27), and a phase angle of $45°$. The frequency consists of a constant value, carrier and modulation signal, as shown in Figure 4.4b.

$$A(t) = 100 + 10 \cdot \sin(2\pi f_v t) \tag{4.27a}$$

$$f(t) = 50 + 0.1 \cdot \sin(2\pi f_m t) \cdot \sin(2\pi f_c t) \tag{4.27b}$$

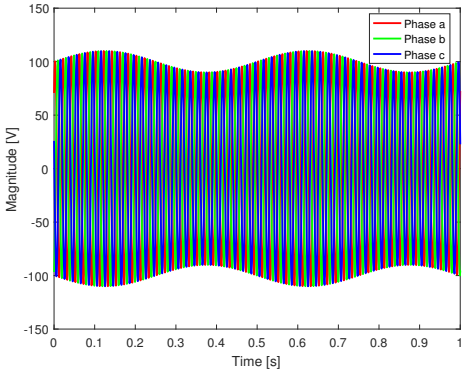

(a) A small section of the three-phase voltages.

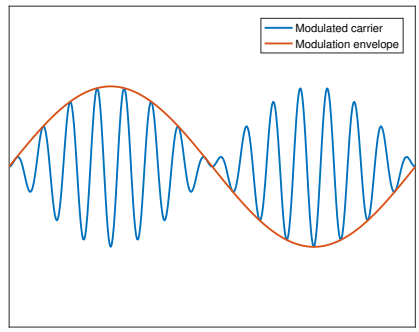

(b) Shape of the frequency around the constant value.

Figure 4.4: Three-phase voltages and frequency.

As shown in Figure 4.5 and Figure 4.6 the EKF and UKF are both clearly able to accurately track the time-varying- magnitude and fundamental frequency. Due to the nonlinear variations of the fundamental frequency, the phase angles are not satisfactory tracked as they are oscillating around the reference. This comes from the fact that the model is assuming constant values, and not several time-varying quantities. As the frequency is constantly changing, the phase angle never gets to settle to its correct value.

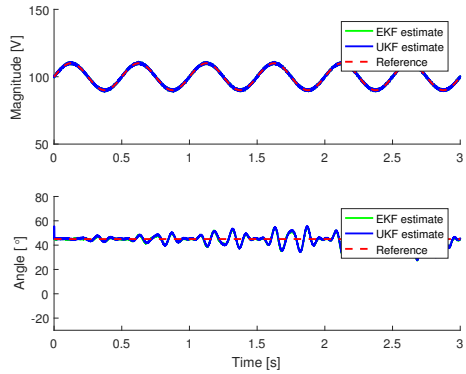

(a) Magnitude and phase angle

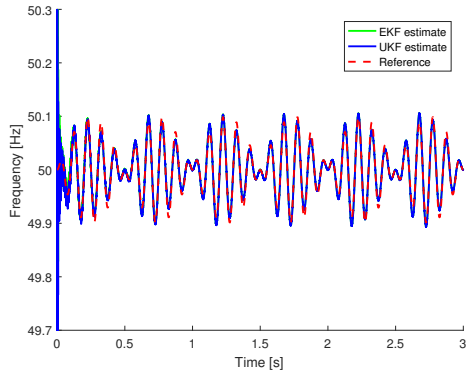

(b) Frequency

Figure 4.5: Tracking of voltages with time-varying amplitude and frequency with $f_v = 2\,Hz$, $f_m = 1\,Hz$, $f_c = 10\,Hz$.

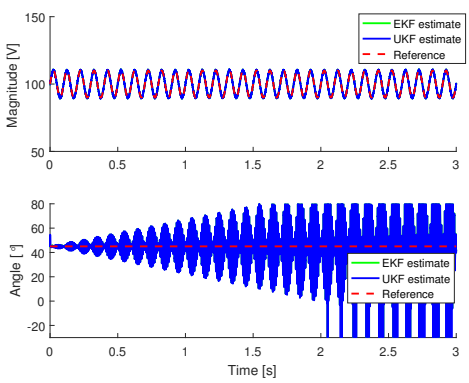

(a) Magnitude and phase angle

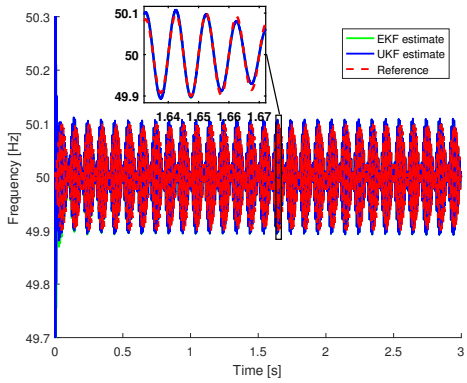

(b) Frequency

Figure 4.6: Tracking of voltages with time-varying amplitude and frequency with $f_v = 10\,Hz$, $f_m = 5\,Hz$, $f_c = 100\,Hz$.

It is found that when the expression $f_v = f_c - f_m \Leftrightarrow f_v = f_m - f_c$ holds, the EKF and UKF fails to track the frequency. This can be observed in Figure 4.7, where the expression holds and the frequency estimates are slowly but surely collapsing. The reasons for this remains unknown, but the author encourages further investigation of this phenomenon as it will not be further studied in this thesis. Also, the author failed to obtain reasonable results for the adaptive UKF in noisy environments, i.e in the environments it is supposed to excel. Further work of this adaptability is suggested for further studies.

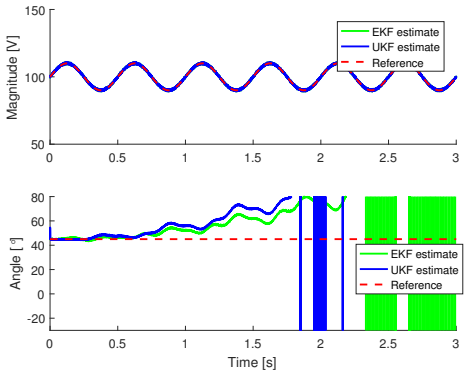

(a) Magnitude and phase angle

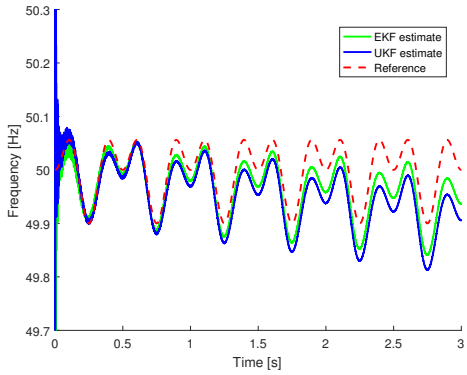

(b) Frequency

Figure 4.7: Tracking of voltages time-varying amplitude and frequency with $f_v = 2\,Hz$, $f_m = 1\,Hz$, $f_c = 3\,Hz$.

Chapter 5

Merging Empirical Mode Decompositon and Kalman Filtering

THE method of combining KFs (UKF will be used), with their inherent real-time properties, and on-line EMD for tracking of instantaneous amplitude and frequency of voltage- and current waveforms in isolated microgrids will here be assessed. Such waveforms are often multicomponent, resulting in the need of decomposition into monocomponents in order to study instantaneous amplitude and frequency. This is a new method proposed by the supervisor and the author. The fundamental difference between this method and the HHT are how the frequencies are calculated.

In this thesis, two different EMD implementations are used. They are implemented as offline algorithms, but assumed to be on-line. One EMD is implemented by the author in Matlab, inspired by [53]. Matlab code for EMD_1 can be found in Appendix B.2 . The other EMD is used as given in [54, 55], also implemented in Matlab. They are denoted as EMD_1 and EMD_2 respectively.

5.1 Single-Phase Systems

FOR real-time EMD+UKF tracking in single-phase microgrids, Figure 5.1 shows a proposed structure. The single-phase voltage $v(t) = v$ is decomposed into monocomponents by a single EMD. The resulting IMFs, IMF_i, $i \in \{1, 2, \ldots, n\}$, and their HT, $\mathscr{H}\{IMF_i\}$, $i \in \{1, 2, \ldots, n\}$ are injected pairwise into independent UKFs. The measurement equation for the uppermost UKF at time step k will be $v_k = IMF_1[k] + j\mathscr{H}\{IMF_1\}[k]$. The same measurement equations with their respective IMFs also yields for UKF $2, ..., n$.

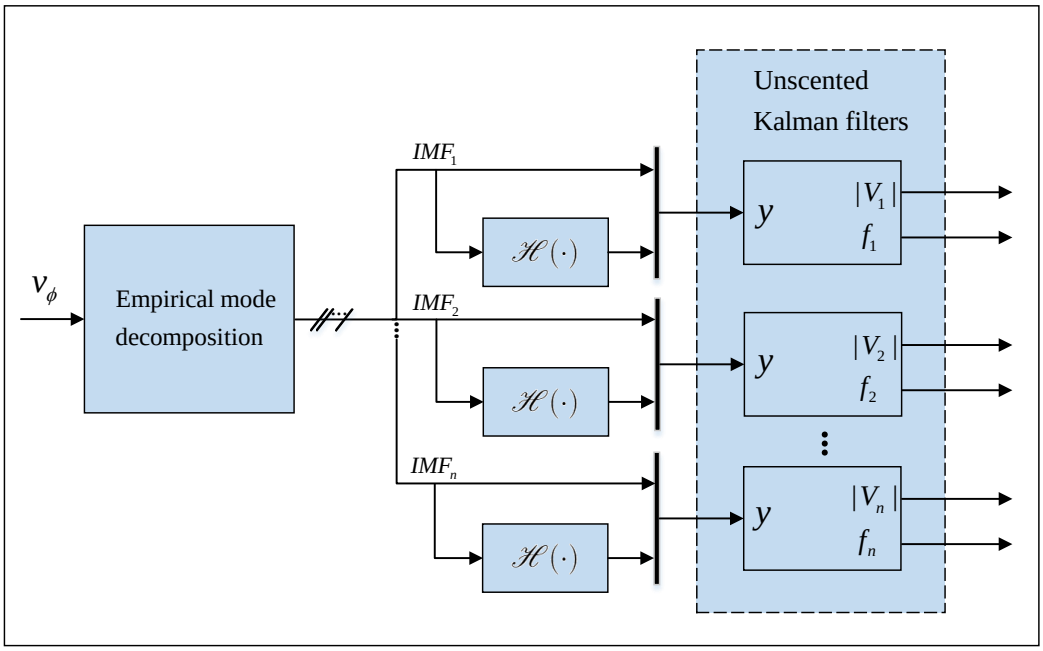

Figure 5.1: Merging of EMD and KF. Single-phase structure.

5.2 Three-Phase Systems

THE EMD+UKF structures for real-time tracking in three-phase systems are shown in Figure 5.2. The main difference between the two structures is that the Clarke transform is done before and after the EMD, and more importantly that structure 2 needs two EMDs instead of three. They are expected to have the same accuracy, hence structure 2 is expected to be the preferable choice. Injecting space vectors into the single-phase structure is also possible, but will not be further discussed.

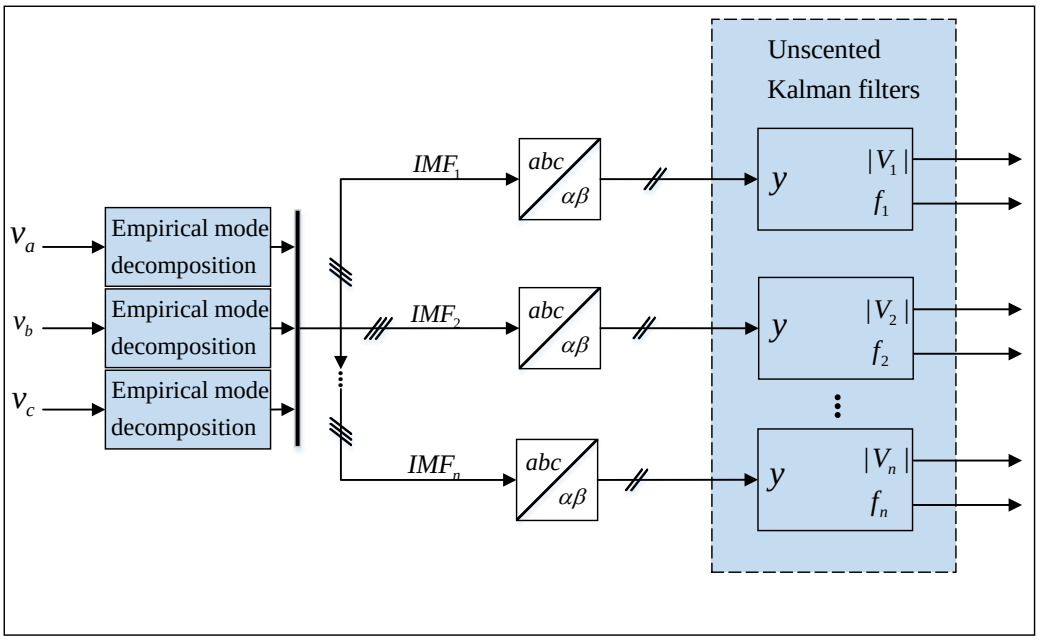

(a) Structure 1

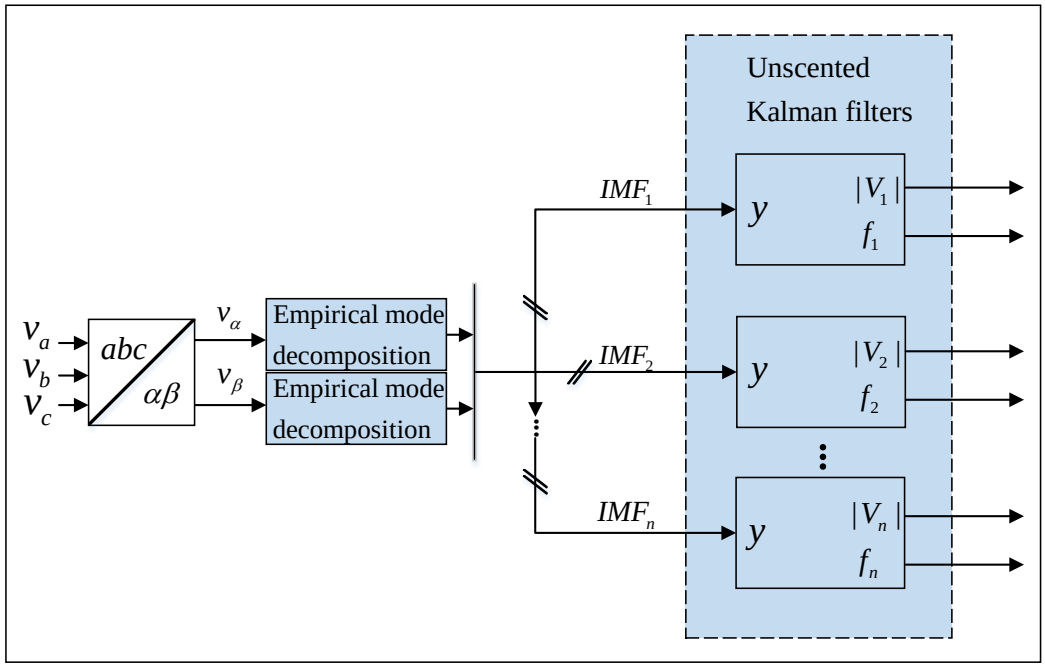

(b) Structure 2

Figure 5.2: Merging of EMD and KF. Three-phase structures.

5.3 Merging Empirical Mode Decompositon and Kalman Filtering - A Validation Study

IN this section it is investigated how the merging of EMD and UKF is performing compared to the UKF. Two different experiments are conducted to reveal the potential of the proposed method and the limitations of the model used in the EKF and UKF. Three-phase structure 1 and EMD_1 is used in this section.

5.3.1 Experiment 1

The EMD+UKF and UKF are subjected to the voltages as given in equation (5.2), with parameter values and tuning as listed in table 5.1. The voltages consists of the sum of two sinusoids with different amplitudes and frequencies. A small section of the waveform of $v_a(t)$ is shown in Figure 5.4a. Figure 5.4b shows how the UKF fails to find the magnitude and frequency in the three-phase system, while the proposed method quickly settles to the reference values, as seen in Figure 5.4c and Figure 5.4d. Additionaly the IMFs and residue can be seen in Figure 5.3. The UKF fails due to a model that is not suitable for the studied signal. Recall the UKF assumes voltages on the form (discrete) $v_k = v_{\alpha,k} + jv_{\beta,k} = V_k \cos(\omega k T_s + \phi_k) + V_k j \sin(\omega k T_s + \phi_k) = V_k e^{j(\omega k T_s + \phi_k)}$. The UKF will try to fit the voltages in equation (5.2) to a model that assumes a balanced three-phase system. As [37] states, the concept of instantaneous frequency loses its meaning when studuying a multicomponent signal.

As the UKF in fact is estimating the magnitude and frequency of the space vector rotating in the complex plane, the EMD is also applied to the space vector of the three-phase system, defined as:

$$\vec{v}(t) = \frac{v_\alpha(t) + v_\beta(t)}{\sqrt{2}}, \tag{5.1}$$

where the dividing by $\sqrt{2}$ is introduced for the space vector and phase voltages to have the same magnitude.

$$v_a(t) = \hat{V}_1 \sin(2\pi f_1 t) + \hat{V}_2 \sin(2\pi f_2 t) \tag{5.2a}$$

$$v_b(t) = \hat{V}_1 \sin(2\pi f_1 t - 120^\circ) + \hat{V}_2 \sin(2\pi f_2 t - 120^\circ) \tag{5.2b}$$

$$v_c(t) = \hat{V}_1 \sin(2\pi f_1 t + 120^\circ) + \hat{V}_2 \sin(2\pi f_2 t + 120^\circ) \tag{5.2c}$$

Experiment 1	
Parameter	**Value**
Simulation time	2 s
Sample time, T_s	$10^{-4}\,s$
Noise variance, $var(v) = E[v^2]$	0
$\hat{V}_1$	$100\,V$
$\hat{V}_2$	$50\,V$
f_1	$35\,Hz$
f_2	$232\,Hz$

(a) Parameters for experiment 1.

UKF tuning	
Parameter	**Value**
$q_{1,1}$	$1 \cdot 10^{-8}$
$q_{2,2}$	$1 \cdot 10^{8}$
R	0.1
α	0.5
β	2
κ	0
P_0^-	$10000 \cdot I_2$
$\hat{x}_0^-$	$\mathbf{0}_{2\times 1}$

(b) UKF tuning in experiment 1.

Table 5.1: Parameters and tuning in experiment 1.

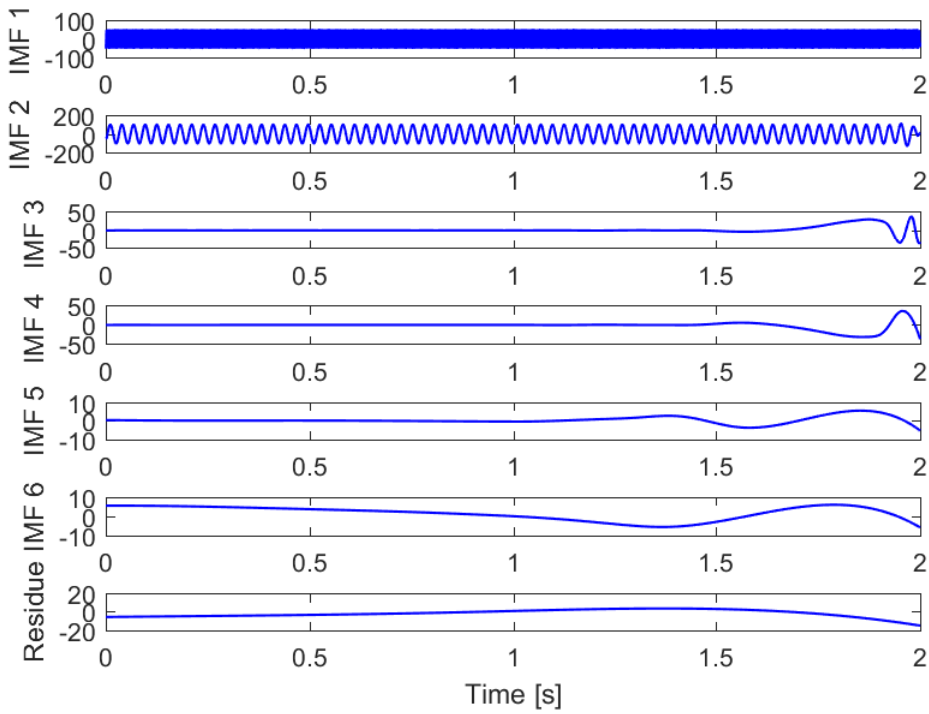

Figure 5.3: The IMFs and residue of the space vector.

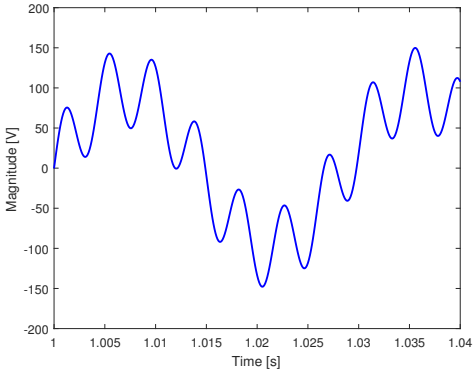

(a) $v_a(t)$, $1s \leq t \leq 1.04s$

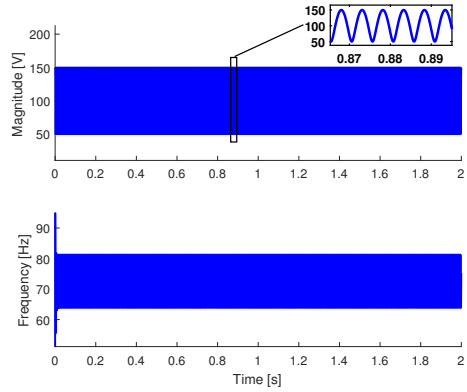

(b) UKF estimate

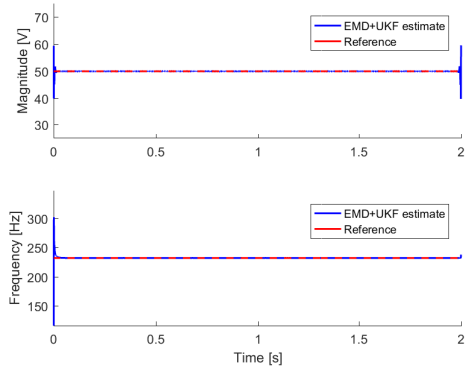

(c) EMD+UKF estimate - IMF 1

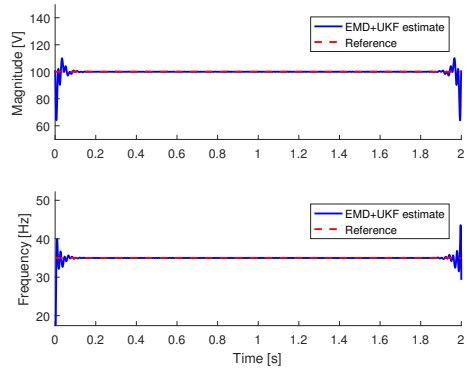

(d) EMD+UKF estimate - IMF 2

Figure 5.4: Experiment 1 results.

5.3.2 Experiment 2

In this experiment the EMD+UKF and UKF are subjected to the three-phase voltages as given in equation (5.5), and with parameter values and tuning as listed in table 5.2. This time, one of the sinusoids consists of a time-varying amplitude and frequency. A small section of the waveform $v_a(t)$, and the different results are shown in Figure 5.6, and the IMFs and residue in Figure 5.5. Again the UKF fails due to an erroneous model, as explained in experiment 1. Also it is found that the EMD+UKF is more accurate, and more suitable for this type of problem, compared to the HHT as can clearly be seen in Figure 5.6d. Due to the time-varying components of f_1, the frequency estimate of the HHT for IMF 2 is found as:

$$f_1(t) = \frac{1}{2\pi}\frac{d\theta_1(t)}{dt} - \frac{df_1(t)}{dt}t, \tag{5.3}$$

due to the fact that

$$\theta_1(t) = 2\pi f_1(t)t + \phi \tag{5.4}$$

$$v_a(t) = \hat{V}_1(t)\sin(2\pi f_1(t)t + 45^\circ) + \hat{V}_2\sin(2\pi f_2 t) \tag{5.5a}$$

$$v_b(t) = \hat{V}_1(t)\sin(2\pi f_1(t)t - 75^\circ) + \hat{V}_2\sin(2\pi f_2 t - 120^\circ) \tag{5.5b}$$

$$v_c(t) = \hat{V}_1(t)\sin(2\pi f_1(t)t + 165^\circ) + \hat{V}_2\sin(2\pi f_2 t + 120^\circ) \tag{5.5c}$$

Experiment 2	
Parameter	**Value**
Simulation time	5 s
Sample time, T_s	$10^{-4}\,s$
Noise variance	$0\,V$
$\hat{V}_1(t)$	$100 + 10\sin(2\pi f_v t)\,V$
$\hat{V}_2$	$50\,V$
$f_1(t)$	$50 + 0.1\sin(2\pi f_m t)sin(2\pi f_c t)\,Hz$
f_2	$250\,Hz$
f_v	$2\,Hz$
f_m	$1\,Hz$
f_c	$10\,Hz$

(a) Parameters for experiment 2.

UKF tuning	
Parameter	**Value**
$q_{1,1}$	$1 \cdot 10^{-8}$
$q_{2,2}$	$1 \cdot 10^{8}$
R	0.1
α	0.5
β	2
κ	0
P_0^-	$10000 \cdot I_2$
$\hat{x}_0^-$	$\mathbf{0}_{2\times 1}$

(b) UKF tuning in experiment 2.

Table 5.2: Parameters and tuning in experiment 2.

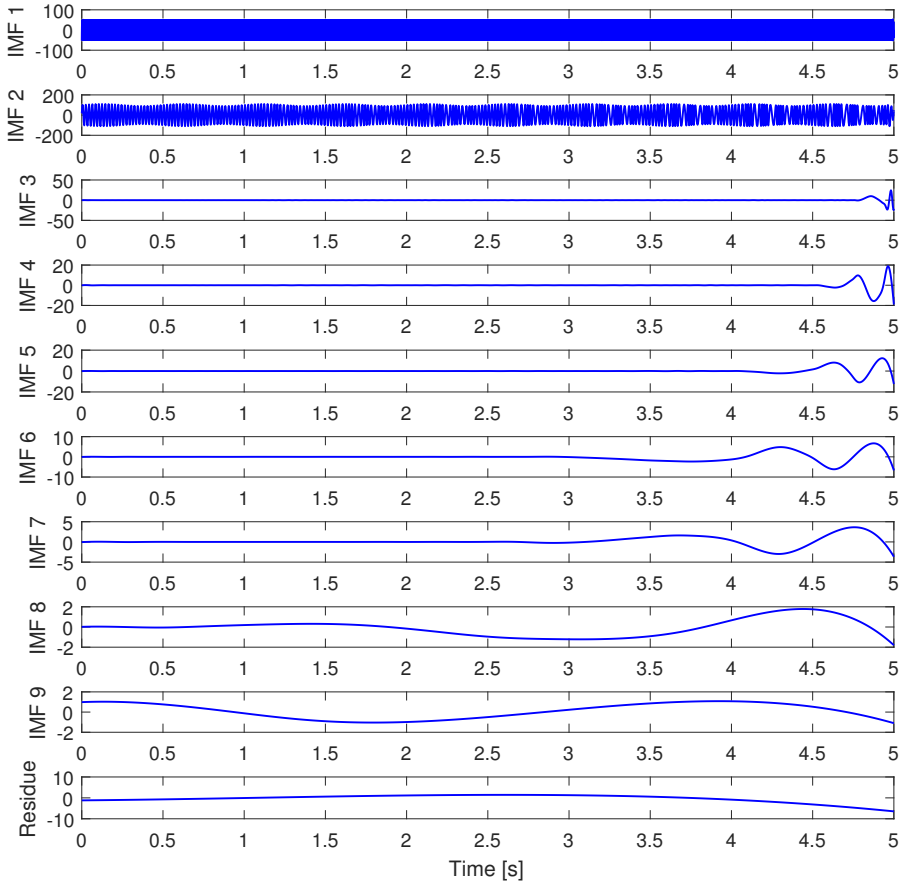

Figure 5.5: The IMFs and residue of the space vector.

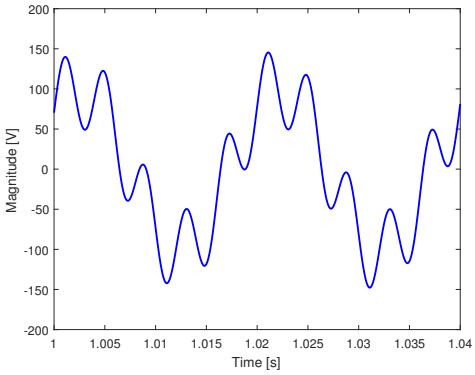

(a) $v_a(t), 1s \leq t \leq 1.04s$

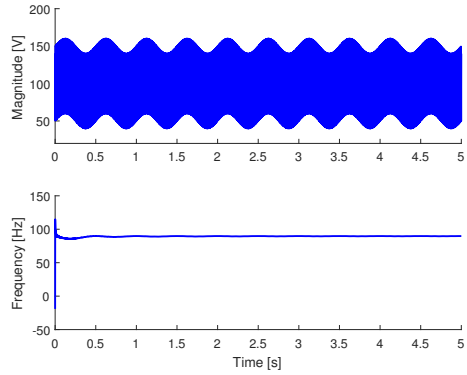

(b) UKF estimate

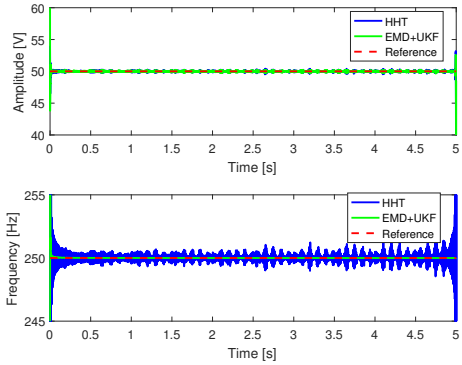

(c) EMD+UKF estimate - IMF 1

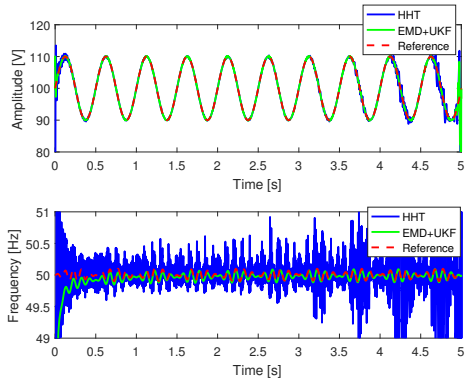

(d) EMD+UKF estimate - IMF 2

Figure 5.6: Experiment 2 results.

Chapter 6

Assessment of Methods for Tracking of Time-Varying Frequencies in real data from a Marine Vessel Power System

In this chapter it is studied how the different tracking methods are able to capture the time-varying fundamental frequency present in the voltages measured on marine vessel power system during sea voyage in rough sea. It is reported in [4, 56] that the time-varying frequency stem from the dynamic load demand in rough sea conditions. The former outlined methods, i.e UKF, HHT and merged EMD and UKF, will be tested with real voltage measurements for 3.33 seconds and 60 seconds (out of 11 minutes) periods. The UKF is chosen over EKF due to marginally better results in preliminary testing. Whether the UKF or EKF should be chosen in real applications should be investigated in each case as they both have their pros and cons as mentioned in section 2.3.2. The UKF is usually preferred over the EKF even though the UKF often has slightly higher computational load, which can be justified by a more robust performance [30]. A small section of the measured line voltages can be seen in Figure 6.1a, where the observant reader may notice some small distortions in the waveforms. Also, defying the shortcomings of Fourier based methods used on time-varying signals, the space vector of the three-phase system is analysed with FFT to serve as a preliminary study, with results as shown in Figure 6.1b. The space vector, $\vec{v}(t)$ is defined as follows:

$$\vec{v}(t) = \frac{v_\alpha(t) + v_\beta(t)}{\sqrt{2}} \tag{6.1}$$

where

$$\begin{bmatrix} v_\alpha(t) \\ v_\beta(t) \end{bmatrix} = \frac{2}{3} \begin{bmatrix} 1 & -\frac{1}{2} & -\frac{1}{2} \\ 0 & \frac{\sqrt{3}}{2} & -\frac{\sqrt{3}}{2} \end{bmatrix} \begin{bmatrix} v_a(t) \\ v_b(t) \\ v_c(t) \end{bmatrix} \tag{6.2}$$

As expected a peak emerges around the fundamental frequency at $50\,Hz$ in the FFT plot. The spikes in the higher frequencies are not easy to interpret, but there are some hints about significant components with frequencies of $850 - 950\,Hz$ and $3.6 - 3.8\,kHz$.

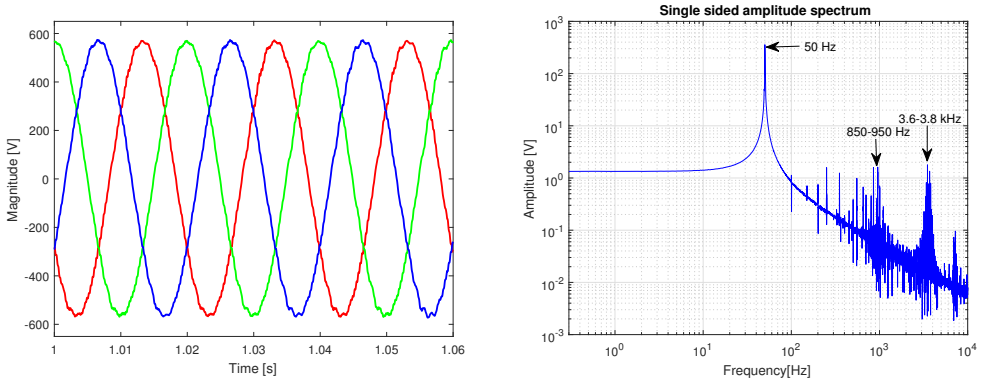

(a) A small section of the measured line voltages.

(b) FFT of the space vector in logarithmic scale.

Figure 6.1: Line voltages and FFT plot.

The UKF is tuned with values as given in table 6.1 for the rest of this chapter. At first glance the UKF may seem hard to tune, but the only tuning knob used is $Q = diag([q_{1,1},\, q_{2,2}])$, while the other tuning knobs are kept constant. Also, a MAF of 800 samples is used on the frequency estimate from the UKF, HHT and merged EMD and UKF. This is done to avoid noisy results due to the derivative in the HHT, i.e $\frac{d\theta}{dt}$, and the aggressively tuned UKF. The UKF is tuned aggressively in order to be able to track the rapid fluctuations in the frequency of the measured voltages. A PLL as in [49] and Figure 2.12a is implemented and used with the purpose of providing a frequency "reference". The Simulink models of the experiment setup, UKF and PLL can be seen in Appendix A.2, with code as included in Appendix B.

UKF tuning	
Parameter	**Value**
$q_{1,1}$	$1 \cdot 10^{-6}$
$q_{2,2}$	$5 \cdot 10^{4}$
R	0.1
α	0.5
β	2
κ	0
P_0^-	$10000 \cdot I_2$
$\hat{x}_0^-$	$\mathbf{0}_{2\times 1}$

(a)
UKF tuning for tracking of IMF 3.

UKF tuning	
Parameter	**Value**
$q_{1,1}$	$1 \cdot 10^{-4}$
$q_{2,2}$	$1 \cdot 10^{2}$
R	0.1
α	0.5
β	2
κ	0
P_0^-	$10000 \cdot I_2$
$\hat{x}_0^-$	$\mathbf{0}_{2\times 1}$

(b)
UKF tuning for tracking of IMF 1 and IMF 2.

Table 6.1: UKF tunings for tracking on the marine vessel.

6.1 3.33 second analysis

THIS section will assess the performance of the former outlined frequency identification methods when analysing the 3.33 first seconds of the measured line voltages on the marine vessel. The space vector is defined as in equation (6.1), and the line voltages are converted to phase voltages to be compliant with the single-phase- and three-phase merged EMD and UKF structures. The IMFs from EMD_1 and EMD_2 are shown in Figure 6.2. It appears to be two high frequencies in addition to the fundamental component. These high frequency components will be further studied in the 60 second chapter. As can be seen in Figure 6.2a the fundamental component, i.e IMF 3 and IMF 4, are split into two or more IMFs. This unwanted mode mixing turned out to be problem when analysing the ship voltages with the EMD. Figure 6.2b shows that the fundamental component is extracted as one IMF, as we want. This is obtained by tuning EMD_2 to low resolution. The low resolution results in a slightly less accurate extraction of IMF 1 and IMF 2. Regardless of slightly lower accuracy, IMF 3 from EMD_2 will be used for most of the results in this section. It would've been possible to use $\sum_{i=1}^{n}\{IMF_i\} + res - IMF_1 - IMF_2$ as estimate of the fundamental component by EMD_1, but is avoided to maintain tracking with no assumptions and a priori knowledge. Using this equation would've assumed only two high frequency components, and the fundamental component, while information about possible lower frequencies would've disappeared into the IMF for the fundamental component.

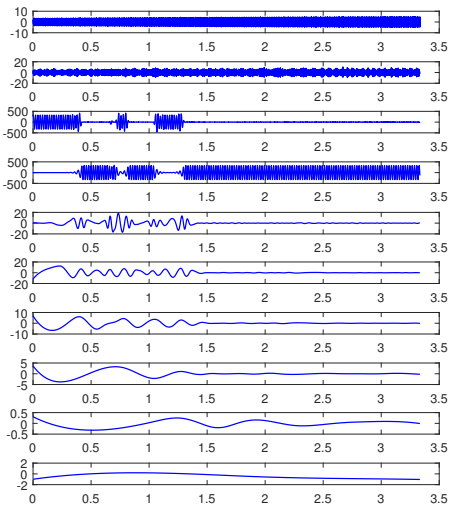

(a) IMFs and residue extracted by EMD_1.

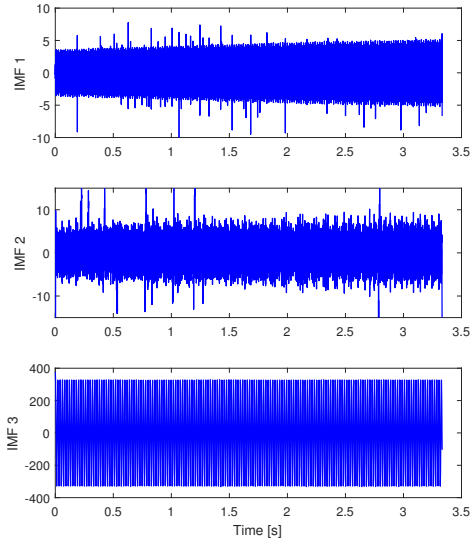

(b) IMFs extracted by EMD_2.

Figure 6.2: IMFs of the 3.33 seconds space vector.

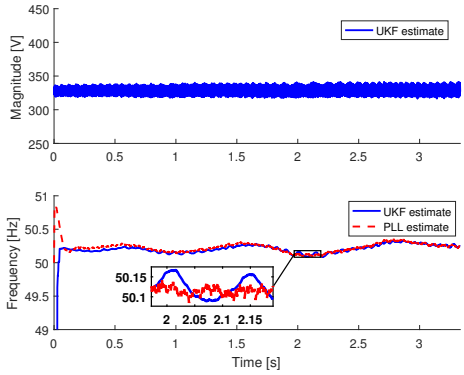

(a) UKF estimation.

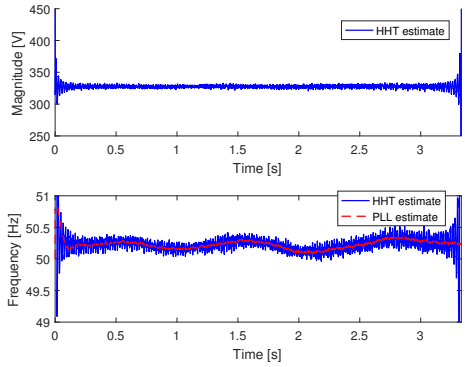

(b) HHT applied to space vector.

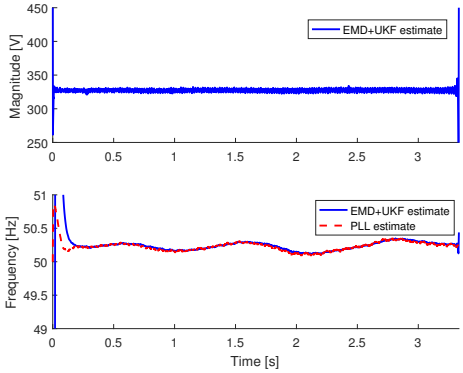

(c) EMD+UKF. Single-phase structure used on phase a.

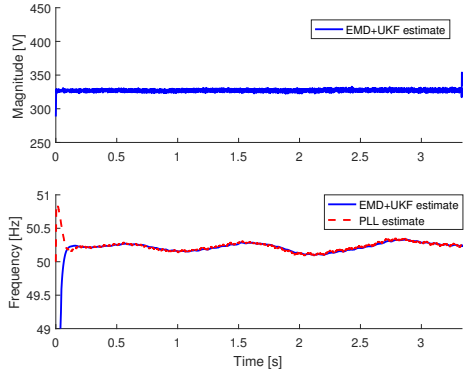

(d) EMD+UKF three-phase structure 1

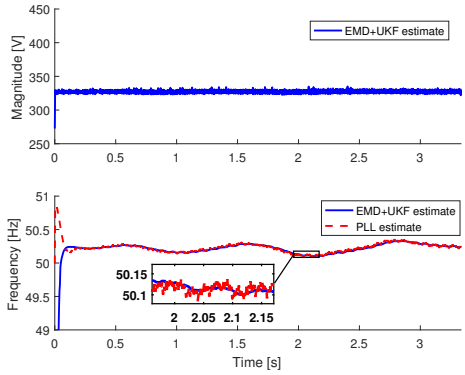

(e) EMD+UKF three-phase structure 2

Figure 6.3: Results using the different methods.

Figure 6.3 shows how the different methods are able to track the fundamental component. It is clear that the three merged EMD and UKF structures provides the most accurate amplitude and frequency estimates. The frequency estimates coincides well with the PLL estimate. The HHT of the space vector also gives acceptable results, but the frequency estimate is quite noisy compared to the frequency estimates of the other methods. The magnitude estimation of the UKF is slightly more inaccurate compared to the other methods. Also, the frequency estimate of the UKF is oscillating around the PLL estimate, as can be observed in Figure 6.3a, and compared to Figure 6.3e. These slight inaccuracies comes from the fact that the UKF is taking the high frequency components into account, while the other methods does not.

6.2 60 second analysis

THE frequency identification methods are now assessed when analysing the 60 first seconds of the measured line voltages on the marine vessel. The same procedures for the space vector, conversion to phase voltages and usage of IMF 3 from EMD_2 applies as in the preceding section.

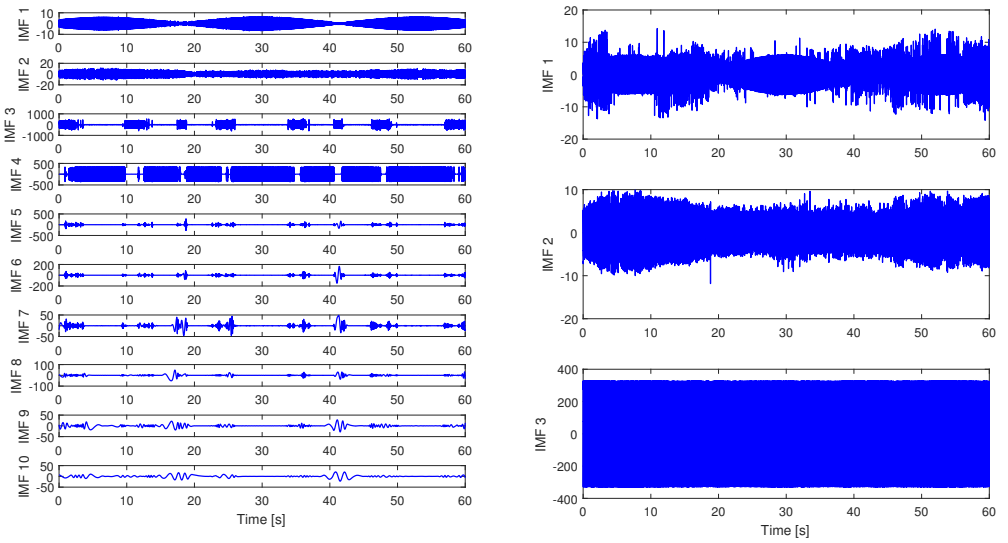

(a) 10 out of 16 IMFs extracted by EMD_1.

(b) IMFs extracted by EMD_2.

Figure 6.4: IMFs of the 60 seconds space vector.

Again, all the methods are managing to track the fundamental component in a good manner. The frequency estimate of the HHT is again more noisy, while the performances of the UKF and merged EMD and UKF are quite similar. Small deviations with respect to the PLL estimate can be observed.

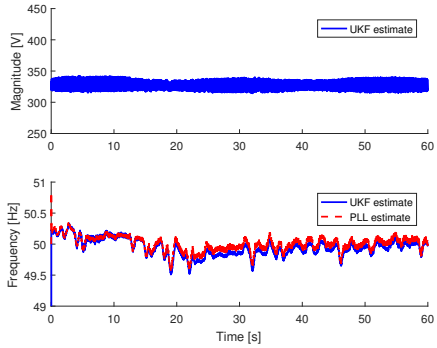

(a) UKF estimation.

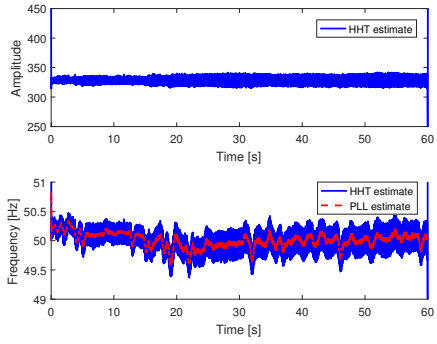

(b) HHT applied to space vector.

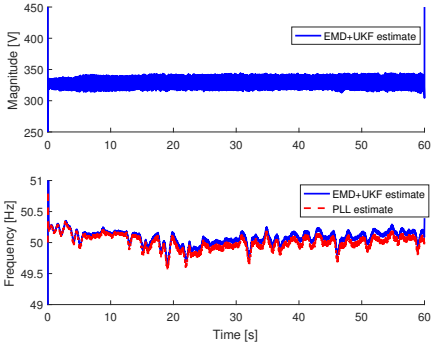

(c) EMD+UKF. Single-phase structure used on phase a.

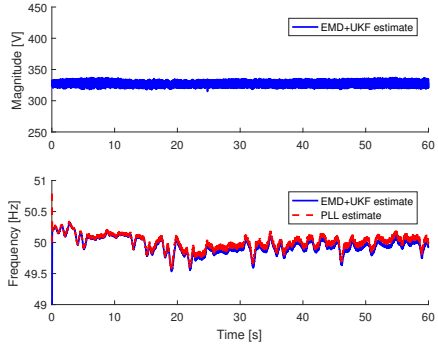

(d) EMD+UKF three-phase structure 1

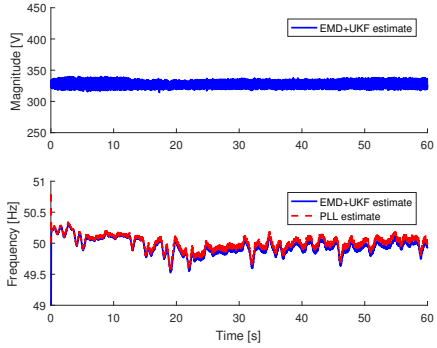

(e) EMD+UKF three-phase structure 2

Figure 6.5: Results using the different methods.

Moving onwards to the two high frequency components, EMD_1 is used due to a more coarse IMF extraction by EMD_2. Due to high computational time, a maximum of 30 sifts per IMF is used. With reasons unknown, the space vector had to be used together with the single-phase structure, as the three-phase structures failed finding the frequency of the high frequency components. Figure 6.6 and Figure 6.7 shows the tracking of the high frequency components, done by HHT and merged EMD and UKF. The magnitudes are in good agreement, while some discrepancies can be observed in the estimated frequencies. Both frequency estimates of IMF 1 rises to approximately $7\,kHz$. The frequency variations between the peaks in IMF 1 can also be observed in the merged EMD and UKF estimate, but are far less visible. From the HHT results it is evident that there is coupling in the oscillations of the frequencies of IMF 1 and IMF 2. Looking at the FFT plot in Figure 6.1b, it is believed that the mentioned higher frequency components in fact are IMF 1 and IMF 2. The interpretation of these results will further be discussed in the next section.

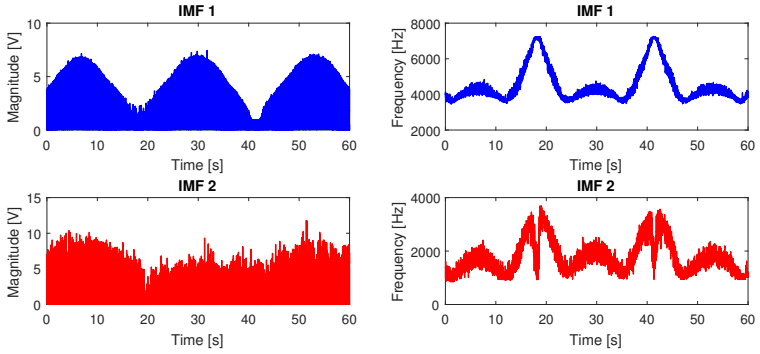

Figure 6.6: The instantaneous amplitude and frequency obtained by HHT for the first and second IMFs.

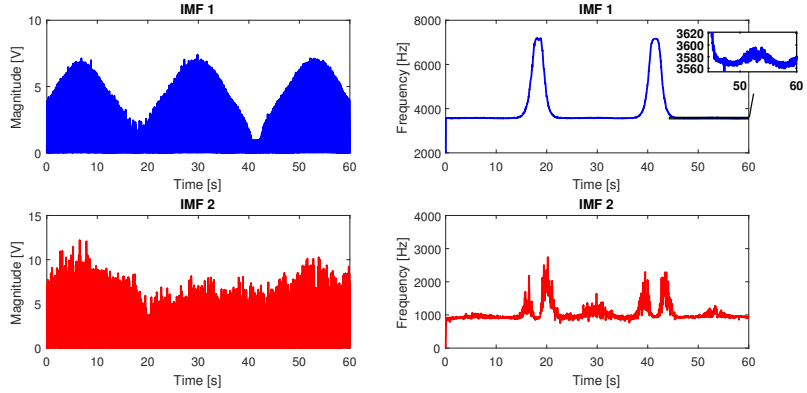

Figure 6.7: The instantaneous amplitude and frequency obtained by the merged EMD and UKF for the two first IMFs.

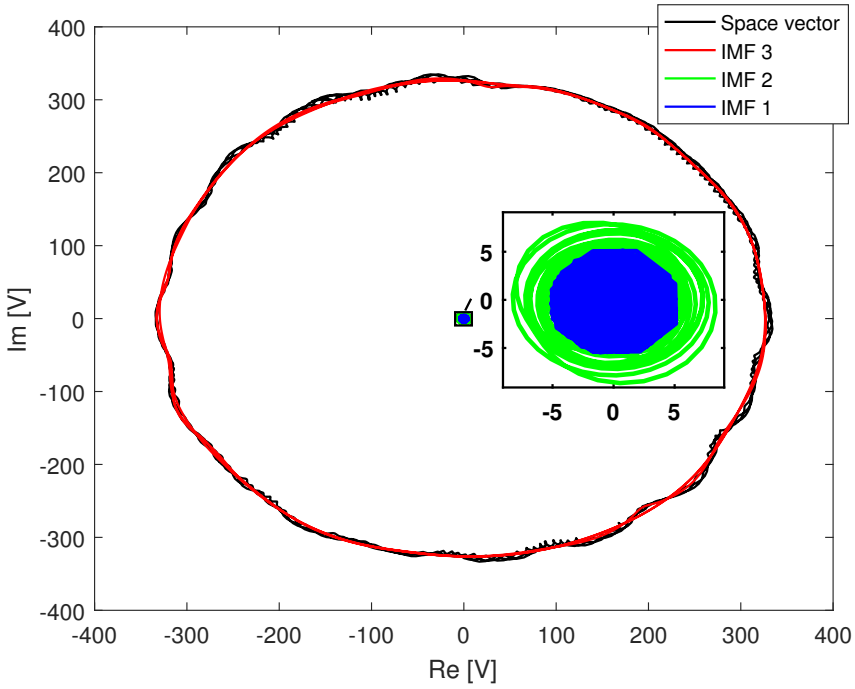

Figure 6.8: The three first IMFs of the space vector, and the space vector it self, plotted for three fundamental periods.

Figure 6.8 shows the trajectories of the three first IMFs in the complex plane, and also the trajectory of the space vector of the voltage measurements. The complex part of the signals are generated by using HT. The chaotic nature of the two first IMFs is evident, while the trajectory of the fundamental component is fairly smooth. The trajectory of the space vector is the trajectory of all the IMFs added together, resulting in the oscillation around the fundamental component, i.e IMF 3.

6.3 Interpreting the Results

REGARDING the tracking of the fundamental component, Figure 6.3 and Figure 6.5 show that the studied methods are managing to track the fundamental component well. Discrepancies are shown between the HHT and merged EMD and UKF in the frequency tracking of IMF 1 and IMF 2, while the estimated amplitudes are coinciding. The reason for this is the fundamental difference between the HT and UKF. By using HT, a signal can be expressed as $y(t) = x(t) + j\mathscr{H}[x(t)] = a(t)e^{j\theta(t)}$, where $a(t)$ is the instantaneous amplitude and $\theta(t)$ is the instantaneous phase. The UKF is relying on a model on the form $y(t) = a(t)e^{j(\omega(t)t+\phi)}$. Both the HT and UKF are finding the amplitude by $a(t) = \sqrt{Re(y(t))^2 + Im(y(t))^2}$, hence the similar results for the amplitudes. The HT finds the frequency by derivating $\theta(t)$, i.e not relying on a model, while the UKF is deriva-

tive free and fits (filters) the measurements to the given state-space model. This results in a more ”noisy” estimate from the HT compared to the UKF.

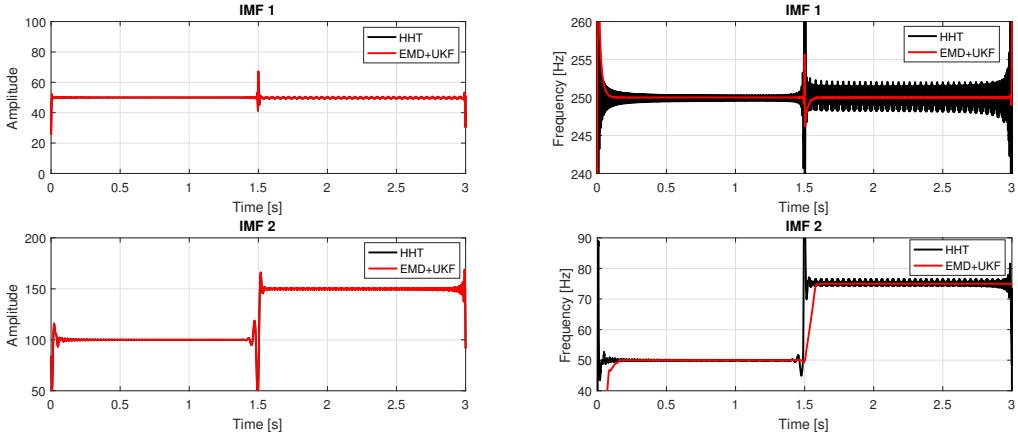

Figure 6.9: Comparison between HHT and merged EMD and UKF

A simple example is conducted where two sinusoids, one constant (IMF 1) and one with steps in amplitude and frequency (IMF 2), are studied by the HHT and merged EMD and UKF. Figure 6.9 illustrates the mentioned differences between the two tools. The amplitudes are coinciding entirely, while the frequency estimates are quite different, due to how they are calculated. It can be seen that both for this synthetic signal, and the real measurements from the marine vessel, that the proposed tool is more accurate under certain circumstances, but no assertions are made for any given signal.

Both the HHT and merged EMD and UKF tracking of IMF 1 and IMF 2, i.e Figure 6.6 and Figure 6.7 reveals that there are some repeating oscillations occurring in the frequencies, and also the amplitude of IMF 1. Figure 6.10 shows sine waves fitted to the observed oscillations in the HHT results. The sine waves are defined as in equation (6.3).

$$x_1(t) = 3.8 + 3 \cdot \sin(2\pi \frac{1}{23.4} \cdot t - 4.3^\circ) \tag{6.3a}$$

$$x_2(t) = 3600 + 600 \cdot \sin(2\pi \frac{1}{23.4} \cdot t - 2.29^\circ) \tag{6.3b}$$

$$x_3(t) = 1000 + 750 \cdot \sin(2\pi \frac{1}{23.4} \cdot t - 2.29^\circ) \tag{6.3c}$$

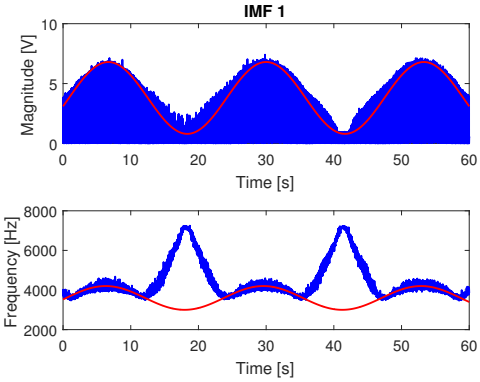

(a) Sine waves ($x_1(t)$ and $x_2(t)$) fitted to the instantaneous amplitude and frequency of IMF 1.

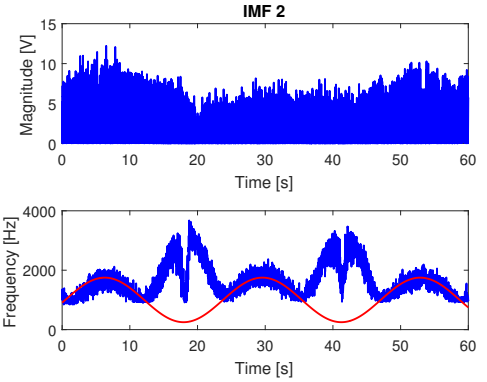

(b) Sine wave ($x_3(t)$) fitted to the instantaneous frequency of IMF 2.

Figure 6.10: Sine fitting to IMF 1.

In mail communication with Tomasz Tarasiuk, the provider of the ship measurements, it was determined that the switching frequency of the converters on the marine vessel was $3.6\,kHz$ [57]. This frequency is clearly visible in Figure 6.7. Interestingly the mean of $x_2(t)$, i.e sine wave fitted to the frequency of IMF 1 found by HHT, is found to be around $3.6\,kHz$. With the mail information in mind it is believed that distortions from the converter switching is found (IMF 1). It is also peculiar to see that the repeating oscillations of the sine waves in equation (6.3) all have the frequency $\frac{1}{23.4}\,Hz$, i.e period of $23.4\,s$. These sine wave are also fitted to IMF 1 and IMF 2 of the full 11 minute measurements, as in Figure 6.11 and Figure 6.12, and are coinciding quite well. Again a maximum of 30 sifts per IMF is used due to a high amount of data points. Up to the date of the master's thesis submission the author is still unsure what these repeating patterns originate from, as they are regarded as too consistent to originate from ocean waves.

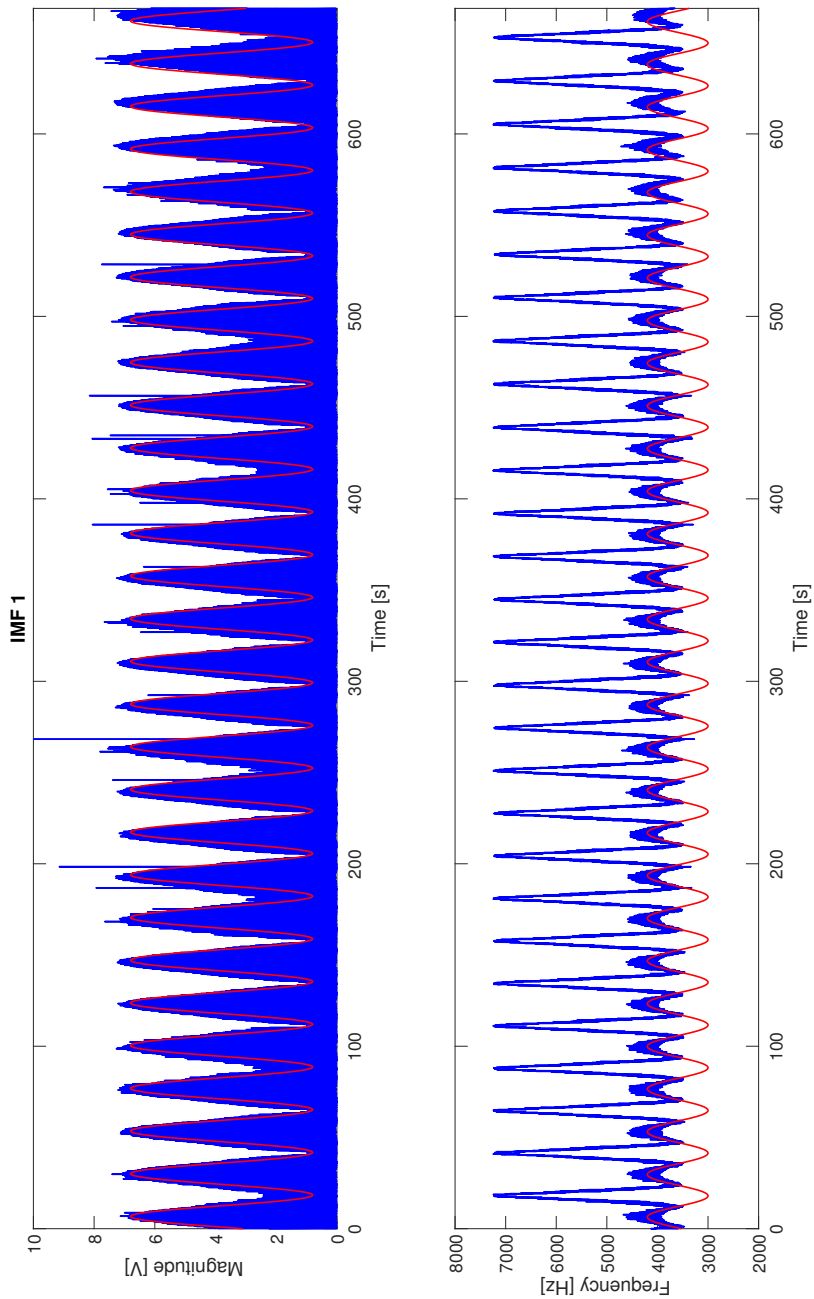

Figure 6.11: Sine wave fitted to the instantaneous amplitude and frequency obtained by HHT.

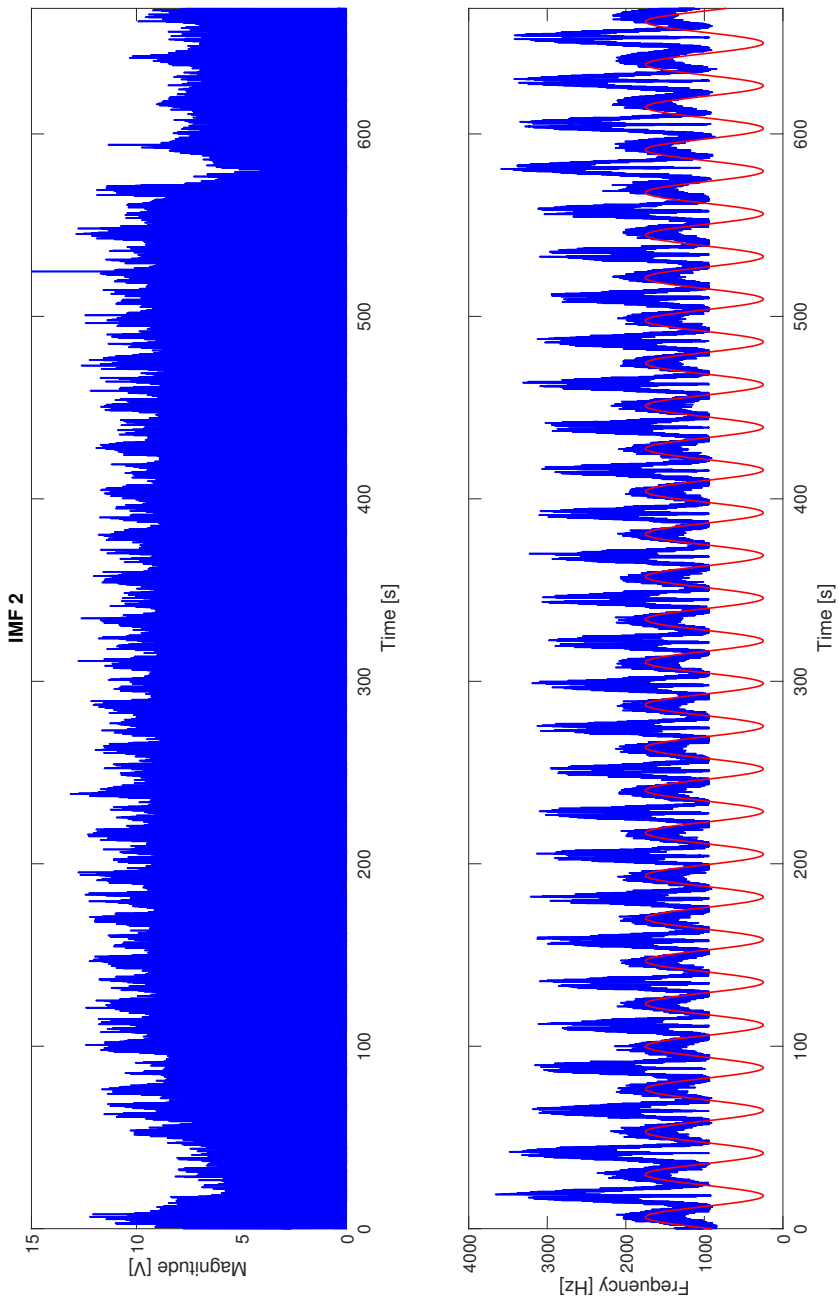

Figure 6.12: Sine wave fitted to the instantaneous frequency obtained by HHT.

Chapter 7

Conclusion and Future Work

In this master's thesis, different methods for tracking of instantaneous frequencies in microgrids have been outlined. The study was motivated from several reports of problems with time-varying frequencies in isolated microgrids [5, 56]. First a brief introduction to microgrids is given, followed by explanation of the most fundamental definitions in electrical power engineering used throughout the thesis. The different KF algorithms, HT, HHT and the PLL are then outlined in a thorough manner. The EKF and UKF, and also the proposed merging of EMD and UKF are initially validated through the analysis of synthetic signals. The EKF and UKF manages to track steps in magnitude, phase and frequency efficiently. It was also shown that the EKF and UKF are able to track signals with time-varying magnitude and frequency, with the exception of a few specific cases. The proposed structures of merged EMD and UKF are presented in chapter 5. The initial analysis of synthetic signals proved the proposed method to be powerful for tracking of instantaneous amplitude and frequency of multicomponent signals with several time-varying monocomponents, even superior to the HHT in that given case. It also showed that the study of instantaneous frequency loses its meaning when considering multicomponent signals [37].

Ultimately, voltage measurements from a marine vessel power system during sea voyage are analysed with the different tracking methods. The UKF, HHT and merged EMD and UKF all proved to be suitable methods for tracking the variations of the fundamental frequency on the vessel, but the proposed method of merging EMD and UKF proved to give slightly better results. The EMD also found additional high frequency components, where one of them are believed to be the switching frequency of the converters. Interesting repeating waveforms are revealed in the high frequency components.

Some problems and interesting findings have been found and left unanswered during the work of this master's thesis. The following work for future papers and master's theses are proposed:

- The EKF and UKF fails estimating signals with magnitudes and frequencies varying with certain frequencies, as explained in section 4.3.2. The reasons for this are not

studied in this thesis.

- The adaptability of the UKF only performed well in noise-free environments, and not in noisy environments where it is supposed to excel and be superior to the regular UKF and EKF [34]. The author strongly encourages this to be further studied so it can be used in the merging with the EMD.
- The EMD implementations used in this thesis are offline. They are assumed to be on-line when used together with the UKF. The author encourages further study involving the development of on-line EMD and its compatibility with the UKF in real-time applications.
- The three-phase structures were not suitable for the study of the high frequency monocomponents on the marine vessel. The single-phase structure and space vector had to be used instead, with reasons unknown to the author.
- Finally, the author strongly suggests to study the origins of the repating waveforms in the instantaneous amplitude and frequency found in the high frequency components of the voltages on the marine vessel.

Bibliography

[1] B. Hillenbrand, G. Kulia, and M. Molinas, "Impact of time varying angular frequency on the separation of instantaneous power components in stand-alone power systems," *6th IEEE International Conference on Clean Electrical Power, Italy*, 2017.

[2] IEEE Standard 519, "IEEE recommended practice and requirements for harmonic control in electric power systems," New York, IEEE Power Energy Society, 2014.

[3] IEC Standard 61000-4-7, "General guide on harmonics and inter-harmonics measurements and measuring instruments for power supply networks and attached devices used for the measurements."

[4] T. Tarasiuk, "Angular frequency variations at microgrids and its impact on measuring instruments performance," *IET Generation, Transmission & Distribution*, vol. 10, No.13, pp. 3234–3240, 2016.

[5] G. Kulia, M. Molinas, L. Lundheim, and B. B. Larsen, "Towards a real-time measurement platform for microgrids in isolated communities," *Humanitarian Technology: Science, Systems and Global Impact 2016, HumTech2016*, vol. 159, pp. 94–103, 2016.

[6] Office of Electricity Delivery and Energy Reliability Smart Grid R&D Program. Summary Report: 2012 DOE Microgrid Workshop. (2012, July 30-31). [Online]. Available: http://energy.gov/sites/prod/files/2012%20Microgrid%20Workshop%20Report%2009102012.pdf

[7] Microgrid Institute. About Microgrids. (2014). [Online]. Available: http://www.microgridinstitute.org/about-microgrids.html

[8] O.-M. Midtgård, "Introduction to a microgrid with a dc bus," Lecture, Norwegian University of Science and Technology, 2016.

[9] C. A. Caizares, "Trends in microgrid control," *IEEE Transactions on Smart Grid*, vol. 5, No.4, pp. 1905–1919, 2014.

[10] N. Mohan, T. M. Undeland, and W. P. Robbins, *Power Electronics - Converters, Applications, and Design*, 3rd ed. Hoboken, NJ: Wiley, 2003.

[11] A. A. Girgis, W. B. Chang, and E. B. Makram, "A digital recursive measurement scheme for on-line tracking of power system harmonics," *IEEE Transactions on Power Delivery*, vol. 6, no. 3, pp. 1153–1160, 1991.

[12] E. Gunther, "Harmonic and interharmonic measurement according to IEEE 519 and IEC 61000-4-7," *Transmission and Distribution Conference and Exhibition, 2005/2006 IEEE PES*, 2006.

[13] J. Cooley, P. Lewis, and P. Welch, "Historical notes on the fast fourier transform," *IEEE Transactions on Audio and Electroacoustics*, vol. 15, No.2, pp. 76–79, 1967.

[14] E. Clarke, W. C. Duesterhoeft, and M. W. Schulz, "Determination of instantaneous currents and voltages by means of alpha, beta, and zero components," *Transactions of the American Institute of Electrical Engineers*, vol. 70, No.2, pp. 1248–1255, 1951.

[15] C. L. Fortescue, "Method of symmetrical co-ordinates applied to the solution of polyphase networks," *Transactions of the American Institute of Electrical Engineers*, vol. XXXVII, no. 2, pp. 1027–1140, 1918.

[16] M. S. Reza, M. Ciobotaru, and V. G. Agelidis, "Power quality analysis using piecewise adaptive prony's method," *2012 IEEE International Conference on Industrial Technology*, 2012.

[17] M. S. Sachdev and M. M. Giray, "A least error squares technique for determining power system frequency," *IEEE Transactions on Power Apparatus and Systems*, vol. PAS-104, No. 2, pp. 437–444, 1985.

[18] A. K. Pradhan, A. Routray, and A. Basak, "Power system frequency estimation using least mean square technique," *IEEE Transactions on Power Delivery*, vol. 20, No. 3, pp. 1812–1816, 2005.

[19] P. Handel and A. Nehorai, "Tracking analysis of an adaptive notch filter with constrained poles and zeros," *IEEE Transactions on Signal Processing*, vol. 42, No. 2, pp. 281–291, 1994.

[20] M. Mojiri, M. Karimi-Ghartemani, and A. Bakhshai, "Estimation of power system frequency using an adaptive notch filter," *IEEE Transactions on Instrumentation and Measurement*, vol. 56, No. 6, pp. 2470 – 2477, 2007.

[21] V. V. Terzija, M. B. Djuric, and B. D. Kovacevic, "Voltage phasor and local system frequency estimation using newton type algorithm," *IEEE Transactions on Power Delivery*, vol. 9, No. 3, pp. 1368 – 1374, 1994.

[22] J. Yang, H. Xi, and W. Guo, "Robust modified newton algorithm for adaptive frequency estimation," *IEEE Signal Processing Letters*, vol. 14, No. 11, pp. 879–882, 2007.

[23] A. A. Girgis and R. G. Brown, "Application of kalman filtering in computer relaying of power systems," *IEEE Transactions on Power Apparatus and Systems*, vol. PAS-100, No. 7, pp. 3387–3397, 1981.

[24] A. A. Girgis and T. L. D. Hwang, "Optimal estimation of voltage phasors and frequency deviation using linear and non-linear kalman filtering: Theory and limitation," *IEEE Transactions on Power Apparatus and Systems*, vol. PAS-103, No. 10, pp. 2943–2951, 1981.

[25] J. A. R. Macias and A. G. Exposito, "Self-tuning of kalman filters for harmonic computation," *IEEE Transactions on Power Delivery*, vol. 21, no. 1, pp. 501–503, 2006.

[26] M. Sun and Z. Sahinoglu, "Extended kalman filter based grid synchronization in the presence of voltage unbalance for smart grid," *Innovative Smart Grid Technologies (ISGT), 2011 IEEE PES*, pp. 1–4, 2011.

[27] P. Dash, A. Pradhan, and G. Panda, "Frequency estimation of distorted power system signals using extended complex kalman filter," *IEEE Transactions on Power Delivery*, vol. 14, No.3, pp. 761–766, 1999.

[28] B. F. La Scala and R. R. Bitmead, "Design of an extended kalman filter frequency tracker," *IEEE Transactions on Signal Processing*, vol. 44, No.3, pp. 739–742, 1996.

[29] A. T. Pham, G. Hermann, and P. Wira, "A new state-space for unbalanced three-phase systems: Application to fundamental frequency tracking with kalman filtering," *IEEE Transactions on Signal Processing*, vol. 44, No.3, pp. 739–742, 2016.

[30] S. Jafarzadeh, C. Lascu, and M. S. Fadali, "State estimation of induction motor drives using the unscented kalman filter," *IEEE Transactions on Industrial Electronics*, vol. 59, No.11, pp. 4207–4216, 2012.

[31] R. E. Kalman, "A new approach to linear filtering and prediction problems," *Transactions of the ASME–Journal of Basic Engineering*, vol. 82D, pp. 35–45, 1960.

[32] R. G. Brown and P. Y. C. Hwang, *Introduction to Random Signals and Applied Kalman Filtering With Matlab Exercises*, 4th ed. Hoboken, NJ: Wiley, 2012.

[33] D. Simon, *Optimal State Estimation: Kalman, H∞, and Nonlinear Approaches*. Hoboken, NJ: Wiley, 2003.

[34] P. Dash, S. Hasan, and B. Panigrahi, "Adaptive complex unscented kalman filter for frequency estimation of time-varying signals," *IET Science, Measurement & Technology*, vol. 4, No.2, pp. 93–103, 2010.

[35] E. Wan and R. V. D. Merwe, "The unscented kalman filter for nonlinear estimation," *Adaptive Systems for Signal Processing, Communications, and Control Symposium 2000*, 2000.

[36] S. L. Hahn, *Hilbert transforms in signal processing*. Boston: Artech House, 1996.

[37] B. Boashash, "Estimating and interpreting the instantaneous frequency of a signal–part 1: Fundamentals," *Proceedings of the IEEE*, vol. 80, No.4, pp. 3234–3240, 1992.

[38] G. Kulia, M. Molinas, and L. Lundheim, "Tool for detecting waveform distortions in inverter-based microgrids: A validation study," *Global Humanitarian Technology Conference (GHTC), 2016*, 2017.

[39] M. Molinas, G. Kulia, and O. B. Fosso, "Instantaneous frequency in electric power systems," 2016.

[40] Y. Hong and Y. Bao, "FPGA implementation for real-time empirical mode decomposition," *IEEE Transactions on Instrumentation and Measurement*, vol. 61, No.12, pp. 3175–3184, 2012.

[41] R. Fontugne, P. Borgnat, and P. Flandrin, "Online empirical mode decomposition," 2017.

[42] S. Shukla, S. Mishra, B. Singh, and S. Kumar, "Implementation of empirical mode decomposition based algorithm for shunt active filter," *IEEE Transactions on Industry Applications*, vol. PP, No.99, 2017.

[43] T. Abdel-Galil, E. El-Saadany, and M. Salama, "Online tracking of voltage flicker utilizing energy operator and hilbert transform," *IEEE Transactions on Power Delivery*, vol. 19, No.2, pp. 861–867, 2004.

[44] F. Zhong-Sheng and X. Nan, "An analysis of various methods for computing the envelope of a random signal," *Applied Ocean Research*, vol. 17, No.1, pp. 9–19, 1995.

[45] T. W. Parks and C. S. Burrus, *Digital Filter Design*. New York: Wiley, 1987.

[46] N. E. Huang, Z. Shen, S. R. Long, M. C. Wu, H. H. Shih, Q. Zheng, N. Yen, C. C. Tung, and H. H. Liu, "The empirical mode decomposition and the hilbert spectrum for nonlinear and non-stationary time series analysis," *Proceedings of the Royal Society of London A: Mathematical, Physical and Engineering Sciences*, vol. 454, pp. 903–995, 1998.

[47] V. Kaura and V. Blasko, "Operation of a phase locked loop system under distorted utility conditions," *IEEE Transactions on Industry Applications*, vol. 33, No. 1, pp. 58–63, 1997.

[48] F. Blaabjerg, R. Teodorescu, M. Liserre, and A. V. Timbus, "Overview of control and grid synchronization for distributed power generation systems," *IEEE Transactions on Industrial Electronics*, vol. 53, No. 5, pp. 1398–1409, 2006.

[49] S. D'Arco, J. A. Suul, and M. Molinas, "Implementation and analysis of a control scheme for damping of oscillations in vsc-based hvdc grids," *16th International Power Electronics and Motion Control Conference and Exposition*, 2014.

[50] R. H. Park, "Two-reaction theory of synchronous machines," *Transactions of the American Institute of Electrical Engineers*, vol. 48, No. 3, pp. 716–727, 1929.

[51] H. J. Helle, "Design and Performance Analysis of a Kalman Filter for Harmonics Tracking in Distorted Power Systems," 2016, Norwegian University of Science and Technology, Department of Engineering Cybernetics- Specialization Project.

[52] A. K. Broen, M. Amin, E. Skjong, and M. Molinas, "Instantaneous frequency tracking of harmonic distortions for grid impedance identification based on kalman filtering," *2016 IEEE 17th Workshop on Control and Modeling for Power Electronics (COMPEL)*, 2016.

[53] Alan Tan. Hilbert-Huang Transform. (2008). [Online]. Available: https://se.mathworks.com/matlabcentral/fileexchange/19681-hilbert-huang-transform

[54] Manuel Ortigueira. Empirical Mode Decomposition. (2008). [Online]. Available: https://se.mathworks.com/matlabcentral/fileexchange/21409-empirical-mode-decomposition

[55] R. Rato, M. Ortigueira, and A. Batista, "On the HHT, its problems, and some solutions," *Mechanical Systems and Signal Processing 22 (2008)*, vol. 22, No.6, pp. 1374–1394, 2008.

[56] J. Mindykowski and T. Tarasiuk, "Problem of power quality in the wake of ship technology development," *Ocean Engineering*, vol. 107, pp. 108–117, 2015.

[57] T. Tarasiuk, private communication, 2017.

Appendices

Appendix A

Simulink Models

THIS appendix includes some of the most significant models implemented in Simulink.

A.1 Tracking in Three-Phase Test System

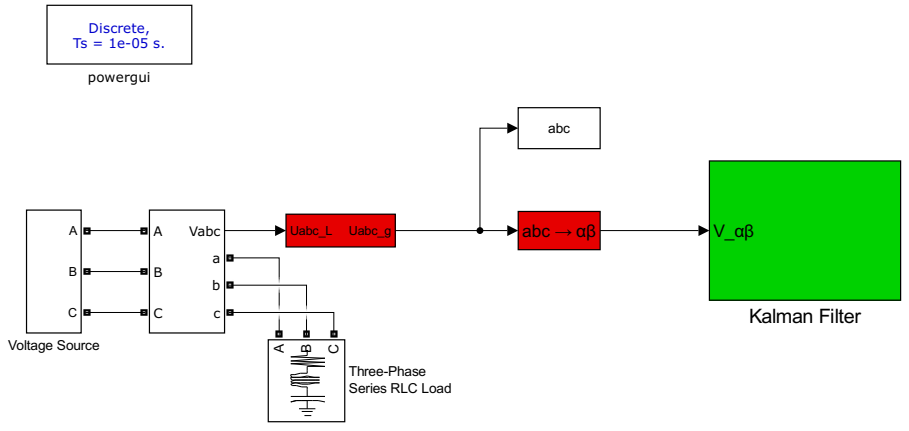

Figure A.1: Implementation of the three-phase test system in Simulink.

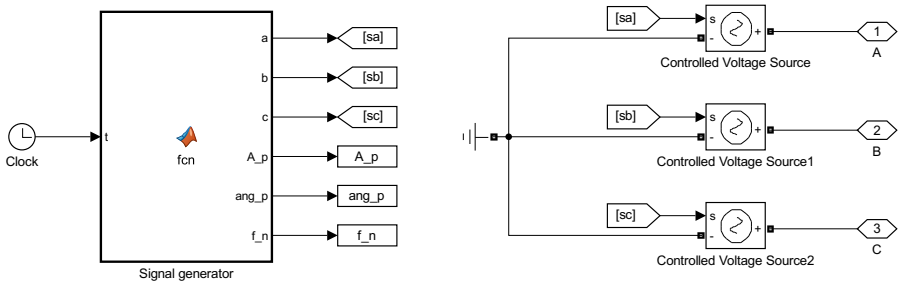

Figure A.2: Implementation of three-phase voltage source in Simulink.

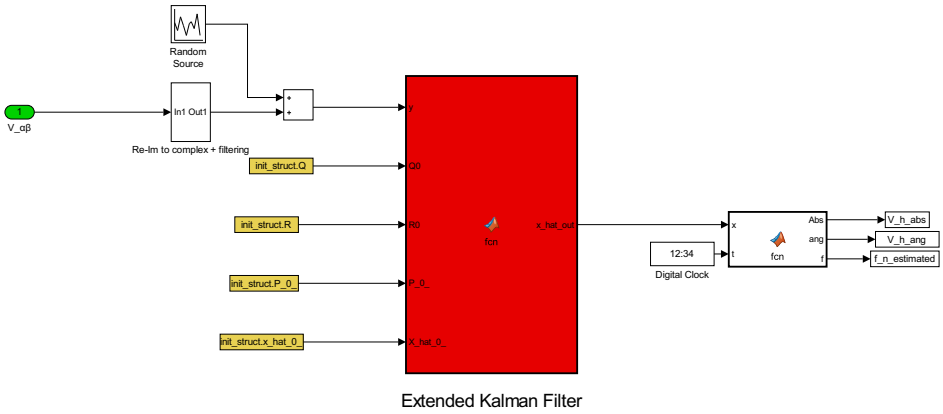

Figure A.3: Implementation of the extended Kalman filter in the test system.

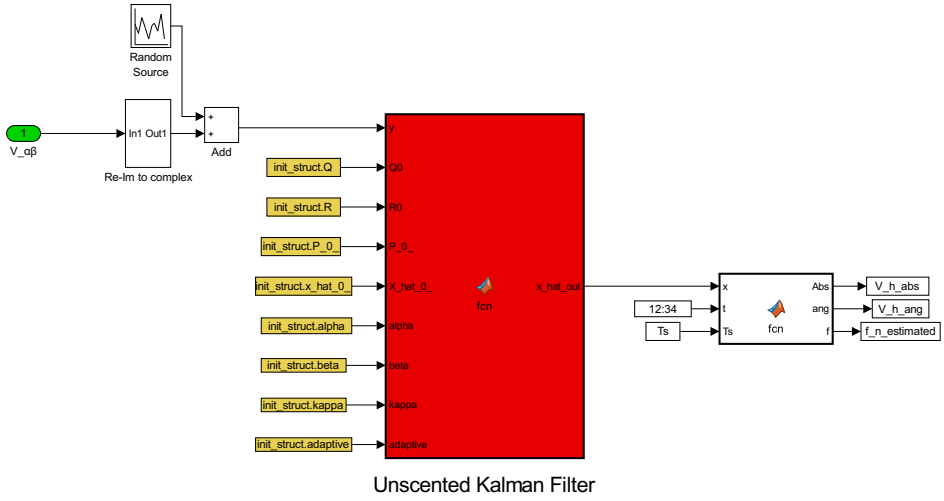

Figure A.4: Implementation of the unscented Kalman filter in the test system.

A.2 Tracking in Marine Vessel Power System

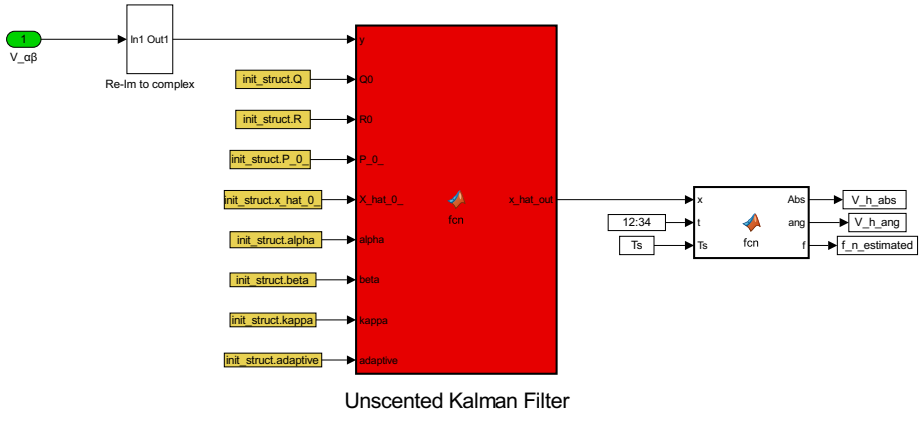

Figure A.5: Implementation of the unscented Kalman filter for tracking on the marine vessel.

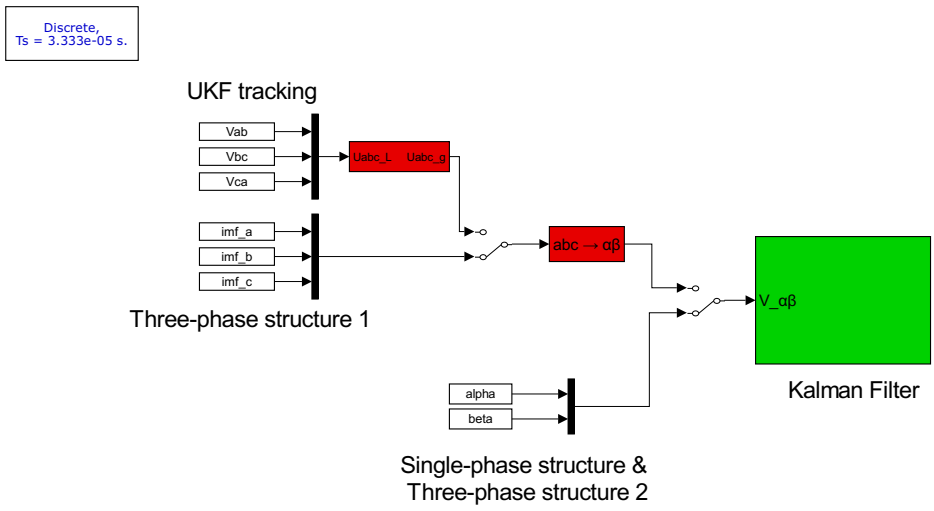

Figure A.6: Implementation of the different tracking methods on the marine vessel.

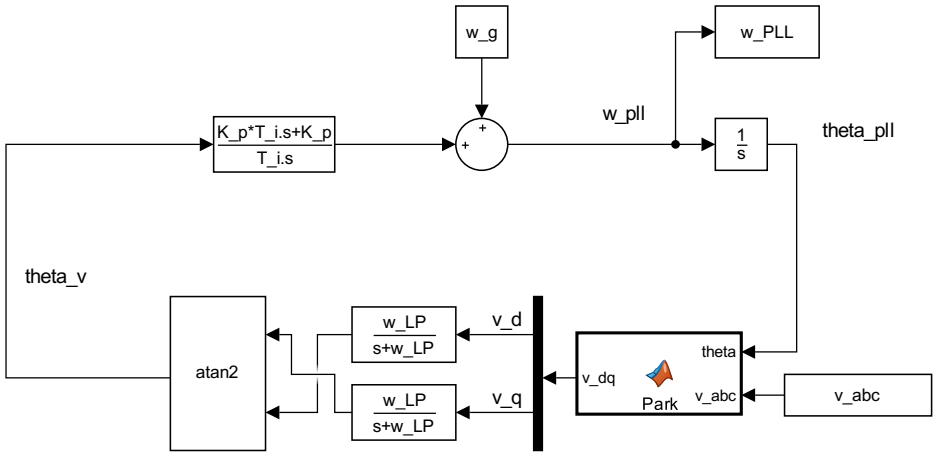

Figure A.7: Implementation of the PLL.

Appendix B

Matlab Code

THE most signicant Matlab scripts and functions are listed in this appendix.

B.1 Voltage Source in the Three-Phase Test System

```
function [a,b,c,A,ang,f]= fcn(t)
    % Making signals for controlled voltage sources
    fv=2;
    fm=1;
    fc=10;

    A=(100+10*sin(2*pi*fv*t));
    ang=45;
    f=50+0.1*sin(2*pi*fm*t)*sin(2*pi*fc*t);

    w=2*pi*f;
    wt=w*t;
    dtr=pi/180;

    a=A(1)*sin(wt+ang*dtr);

    b=A(1)*sin(wt+(ang-120)*dtr);

    c=A(1)*sin(wt+(ang+120)*dtr);
```

B.2 Empirical Mode Decomposition

```
function [imf,res] = emd(x_in,sd)
    %Input:
    %x_in - Input signal
    %sd - Minimum standard deviation between two consecutive siftings.
    %Output:
    %imf - Cell containing the intrinsic mode functions
    %res - The remaining residue after the extraction of intrinsic mode
    %functions

    imf=[];
    x=x_in;
    while monotonic(x)==false
        x_temp=x;
        SD=Inf; % Standard deviation between two consecutive siftings
        while isimf(x_temp)≠true|| sd<SD
            max_spline=makespline(x_temp,true);
            min_spline=makespline(x_temp,false);
            m=(max_spline+min_spline)/2;
            h=x_temp-m;
            SD=sum(abs(x_temp-h).^2)/sum(x_temp.^2);
            x_temp=h;
        end
        imf{end+1}=x_temp;
        x=x-x_temp;
    end
    res=x;
```

```
function b = monotonic(x)
    %Input:
    %x - Input signal
    %Output:
    %b - Boolean. Is monotonic(True=1), is not monotonic(False=0)

    no_max=findpeaks(x,1); % Number of maxima
    no_min=findpeaks(x,0); % Number of minima
    %Return true if there exist both a max and a min
    if(length(no_max)>0&&length(no_min)>0)
        b=false;
    else
        b=true;
    end
```

```
function b = isimf(x)
    %Input:
    %x - Input signal
    %Output:
    %b - Boolean. Is IMF(True=1), is not IMF(False=0)

    u1 = sum(x(1:end-1).*x(2:end) < 0); % Number of zero crossings
```

```
    u2 = length(findpeaks(x,1))+length(findpeaks(x,0)); % Number of ...
        extrema
    if abs(u1-u2) > 1
        b = false;
    else
        b = true;
    end
```

```
function s = makespline(x,is_max)
    %Input:
    %x - Input signal
    %is_max - Extrema boolean. Max(true=1), min(false=0)
    %Output:
    %s - Cubic spline interpolation

    N = length(x);
    if is_max
        p = findpeaks(x,1);
        s = spline([0 p N],[max(x(p(1)),x(1)) x(p) ...
            max(x(p(end)),x(end))],1:N);
    else
        p = findpeaks(x,0);
        s = spline([0 p N],[min(x(p(1)),x(1)) x(p) ...
            min(x(p(end)),x(end))],1:N);
    end
```

```
function extrema_index = findpeaks(x,is_max)
    %Input:
    %x - Input signal
    %is_max - Extrema boolean. Max(true=1), min(false=0)
    %Output:
    %extrema_index - Indices of the extrema points

    extrema_index=[];
    peaks=diff(x);
    if is_max
        for i=1:length(peaks)-1
            if peaks(i)==0&&peaks(i+1)<0||peaks(i)>0&&peaks(i+1)<0
                extrema_index=[extrema_index i+1];
            end
        end
    else
        for i=1:length(peaks)-1
            if peaks(i)==0&&peaks(i+1)>0||peaks(i)<0&&peaks(i+1)>0
                extrema_index=[extrema_index i+1];
            end
        end
    end
```

B.3 Calculation of Instantaneous Amplitude and Frequency

```
function [H,A,f]=process_imf(x,Fs)
    %Input:
    %x - Input signal
    %Fs - sampling frequency
    %Output:
    %H - Signal and Hilbert transform of input signal i.e H=x+jH(x)
    %A - Instantaneous amplitude
    %f - instantaneous frequency

    y=hilbert(x);
    H=y;
    A=sqrt(real(y).^2+imag(y).^2); %Instantaneous amplitude

    ang=zeros(1,length(x));

    %Finding the instantaneous phase
    for i=1:length(ang)
        ang(i)=atan(imag(y(i))/real(y(i)));
    end

    f=zeros(1,length(x));
    %Finding the instantaneous frequency
    for i=1:length(f)-1
        f(i)=(ang(i+1)-ang(i))*Fs/(2*pi);
        if(f(i)<0&&i>1)
            f(i)=f(i-1);
        end
    end
```

B.4 Extended Kalman Filter

```
function x_hat_out  = fcn(y,Q0,R0,P_0_,X_hat_0_)

    %=====================Extended Kalman filter ...
        algorithm==========================
    persistent P_ x_hat_ C Q R A

    if isempty(P_) %Initialization
        x_hat_=complex(X_hat_0_);
        P_=complex(P_0_);
        Q=Q0;
        R=R0;
        C=[0 1];
        A=complex(zeros(2,2));
    end

    K=P_*C'*(C*P_*C'+R)^(-1);      %Finding the kalman gain
    x_hat=x_hat_+K*(y-C*x_hat_);   %Updating estimate of x

```

```
18      P=(eye(2)-K*C)*P_*(eye(2)-K*C)'+K*R*K'; %Joseph form,
19
20      x_hat_out=x_hat; %Output from the Kalman filter, estimated x
21
22      %Linearizing around the updated estimate (a posteriori), x_hat
23      A=[1 0;
24         x_hat(2) x_hat(1)];
25
26      %Projecting ahead
27      x_hat_=A*x_hat;
28      P_=A*P*A'+Q;
```

B.5 Unscented Kalman Filter

```
1  function x_hat_out  = ...
       fcn(y,Q0,R0,P_0_,X_hat_0_,alpha,beta,kappa,adaptive)
2
3  %============Adaptive Complex Unscented Kalman filter ...
       algorithm============
4  persistent P x_hat  Q R e n lambda
5  %% Initializing persistent variables
6  if isempty(P)
7      x_hat=complex(X_hat_0_);
8      n=length(x_hat);
9      P=complex(P_0_);
10     Q=complex(Q0);
11     R=complex(R0);
12     e=complex(zeros(1,1));
13     lambda=alpha^2*(n+kappa)-n;
14 end
15 %--------------------------------------------------
16
17 %% Preallocation of matrices used during the algorithm
18 hx_sigma=complex(zeros(1,2*n+1));
19 x_sigma=complex(zeros(n,2*n+1));
20 fx_sigma=complex(zeros(n,2*n+1));
21 y_hat=complex(zeros(1,1));
22 x_hat_=complex(zeros(2,1));
23 P_=complex(zeros(n,n));
24 Py=complex(zeros(1,1));
25 Pxy=complex(zeros(2,1));
26 %--------------------------------------------------
27
28 %% Making sigma points
29 temp=repmat(x_hat,1,2*n);
30 nP=chol((n+lambda)*P)';
31 temp=temp+[nP -nP];
32 x_sigma=[x_hat temp];
33 %--------------------------------------------------
34
35 %% Propagating through nonlinear function f(.)
36 for k = 1:(2*n+1)
37     fx_sigma(:,k) = f(x_sigma(:,k));
```

```
38  end
39  %---------------------------------------------------
40  %% Obtaining the a priori estimate
41  for i=1:(2*n+1)
42      if i==1
43          weight=lambda/(lambda+n);
44      else
45          weight=1/(2*(lambda+n));
46      end
47      x_hat_(1,1)=x_hat_(1,1)+weight*fx_sigma(1,i);
48      x_hat_(2,1)=x_hat_(2,1)+weight*fx_sigma(2,i);
49  end
50  %---------------------------------------------------
51  %% Estimate a priori error covariance
52  for i=1:(2*n+1)
53      if i==1
54          weight=lambda/(lambda+n)+1-alpha^2+beta;
55      else
56          weight=1/(2*(lambda+n));
57      end
58      P_= P_ + weight*((fx_sigma(:,i)-x_hat_)*(fx_sigma(:,i)-x_hat_)');
59  end
60  P_=P_+Q;
61  %---------------------------------------------------
62
63  %% Making new sigma points
64  temp=repmat(x_hat_,1,2*n);
65  nP=chol((n+lambda)*P_)';
66  temp=temp+[nP -nP];
67  x_sigma=[x_hat_ temp];
68  %---------------------------------------------------
69
70  %% Sigma points through nonlinear measurement function h(.)
71  %% and finding the estimated
72  for k = 1:(2*n+1)
73      hx_sigma(:,k) = h(x_sigma(:,k));
74  end
75  for i = 1:(2*n+1)
76      if i==1
77          weight=lambda/(lambda+n);
78      else
79          weight=1/(2*(lambda+n));
80      end
81      y_hat=y_hat+weight*hx_sigma(1,i);
82  end
83  %---------------------------------------------------
84  %% Estimate predicted measurement covariance
85  for i=1:(2*n+1)
86      if i==1
87          weight=lambda/(lambda+n)+1-alpha^2+beta;
88      else
89          weight=1/(2*(lambda+n));
90      end
91      Py= Py + weight*((hx_sigma(:,i)-y_hat)*(hx_sigma(:,i)-y_hat)');
92  end
93  Py=Py+R;
94  %---------------------------------------------------
```

```
95
96  %% Estimate the cross covariance
97
98  for i = 1:(2*n+1)
99      if i==1
100         weight=lambda/(lambda+n)+1-alpha^2+beta;
101     else
102         weight=1/(2*(lambda+n));
103     end
104     Pxy = Pxy + weight*((x_sigma(:,i)-x_hat_)*(hx_sigma(:,i)-y_hat)');
105 end
106 %-----------------------------------------------------
107 %% Finding the kalman gain and updated estimates
108 K=Pxy/Py;
109 x_hat=x_hat_+K*(y-y_hat);
110 P=P_-K*Py*K';
111 P=0.5*(P+P');% Prevent numerical problems
112 %-----------------------------------------------------
113 if adaptive
114     %Adaptive Q
115     psi= x_hat-x_hat_;
116     Q=0.5*(abs(psi(1))^2+abs(psi(2))^2)*eye(2);
117     if (Q(1,1)>10000 || Q(2,2)>10000)
118         Q=1*eye(2);
119     end
120
121     %Adaptive R
122     e_=e;
123     e=y-y_hat;
124     lambda=0.5;
125     R_=R;
126     R=lambda*R_+(1-lambda)*abs(e)*abs(e_);
127 end
128
129 x_hat_out=x_hat;
130 %-----------------------------------------------------
131
132
133
134 function X = f(x)
135     X=complex(zeros(2,1));
136     X(1)=x(1);
137     X(2)=x(1)*x(2);
138
139 function y = h(x)
140     y=x(2);
```

B.6 From Estimated States to Estimated Magnitude, Phase Angle and Frequency

```
1  function [Abs,ang,f] = fcn(x,t,Ts)
2          persistent  f_array MAF_samples
```

```
3
4           if isempty(f_array)
5               MAF_samples=800;
6               f_array=zeros(1,MAF_samples);
7           end
8           k=t/Ts;
9
10          Abs=sqrt(imag(x(2))^2+real(x(2))^2);
11          f=imag(log(x(1)))/(2*pi*Ts);
12
13          if(k<MAF_samples)
14              f_array(k+1)=f;
15          else
16              f_array=[f_array f];
17              f_array=f_array(2:end);
18          end
19          f_MAF=mean(f_array);
20
21          ang=imag(log(x(2)/sqrt(x(2)*x(2)')))-k*f_MAF*2*pi*Ts;
22
23          while (ang>2*pi)||(ang<-2*pi)
24              if(ang>2*pi&&ang>0)
25                  ang=ang-2*pi;
26              elseif(ang<-2*pi&&ang<0)
27                  ang=ang+2*pi;
28              end
29          end
30          ang=(ang+pi/2)*180/pi; % Angle offset
```

B.7 Park Transformation

```
1  function v_dq = Park(theta,v_abc)
2         v_dq=sqrt(2/3)*[cos(theta) cos(theta-2*pi/3) cos(theta+2*pi/3);
3         -sin(theta) -sin(theta-2*pi/3) -sin(theta+2*pi/3)]*v_abc;
```